JGR Solid Earth

RESEARCH ARTICLE
10.1029/2024JB030067

Key Points:

- Seismicity from surface suture to ~70 km depth reveals subducted continuation of Panamá–Chocó Block
- Supraslab, intermediate (70–120 km) depth seismicity occurs in a segment of the forearc immediately adjacent to this continuation
- This intermediate depth seismicity is localized directly above intense slab seismicity, may mark a site of intense fluid release

Supporting Information:

Supporting Information may be found in the online version of this article.

Correspondence to:

B. T. Bishop,
brandon.t.bishop@slu.edu

Citation:

Bishop, B. T., Warren, L. M., Aravena, P., Cho, S., Soto-Cordero, L., Pedraza, P., et al. (2025). The deep lithospheric structure of terrane accretion as revealed through patterns of seismicity associated with the collision of the Panamá–Chocó Block and South America beneath Cauca, Colombia. *Journal of Geophysical Research: Solid Earth*, *130*, e2024JB030067. https://doi.org/10.1029/2024JB030067

Received 2 AUG 2024
Accepted 10 JUN 2025

Author Contributions:

Conceptualization: Brandon T. Bishop, Linda M. Warren
Data curation: Pablo Aravena, Sungwon Cho, Patricia Pedraza, Viviana Dionicio
Formal analysis: Brandon T. Bishop
Funding acquisition: Linda M. Warren
Investigation: Brandon T. Bishop
Project administration: Linda M. Warren
Resources: Linda M. Warren, Patricia Pedraza, Germán A. Prieto, Viviana Dionicio
Supervision: Linda M. Warren
Validation: Pablo Aravena, Sungwon Cho
Visualization: Brandon T. Bishop
Writing – original draft: Brandon T. Bishop

The Deep Lithospheric Structure of Terrane Accretion as Revealed Through Patterns of Seismicity Associated With the Collision of the Panamá–Chocó Block and South America Beneath Cauca, Colombia

Brandon T. Bishop[1], Linda M. Warren[1], Pablo Aravena[1], Sungwon Cho[1], Lillian Soto-Cordero[1], Patricia Pedraza[2], Germán A. Prieto[3], and Viviana Dionicio[2]

[1]Saint Louis University, Saint Louis, MO, USA, [2]Servicio Geológico Colombiano, Bogotá, Red Sismológica Nacional de Colombia, Bogotá, Colombia, [3]Departamento de Geociencias, Universidad Nacional de Colombia, Bogotá, Colombia

Abstract The Cauca region is the only documented site in the world where extensive intermediate depth seismicity occurs over multiple decades above a subducting slab. Here, the subducting Nazca oceanic plate descends beneath a mosaic of terranes derived from the Caribbean plate and accreted to continental South America from the Cretaceous to the present. Through relative relocation of >6,000 earthquakes from 2010 to 2019 we show that seismic activity within the Nazca slab is concentrated immediately inboard of the most recently accreted terrane (the Panamá–Chocó Block) and that supraslab seismicity is occurring within the subducted continuation of this terrane. The deepest extent of this seismicity occurs only within the Colombian forearc and a gap in the active volcanic arc, indicating that the continuation of this terrane at depth has perturbed the thermal structure of the subduction zone. This perturbation is likely what permits brittle failure to occur above the slab. Within the context of the long-term evolution of the Colombian subduction zone, this seismicity must represent either a transient phenomenon as the continuation of the Panamá–Chocó Block warms and becomes incorporated into the convecting mantle wedge or a site where fluids released by the subducting Nazca slab have been focused, promoting hydrofracture. While additional tests are necessary to distinguish between these possibilities, seismicity within the Nazca slab is most intense directly beneath the locations where supraslab seismicity is concentrated, consistent with hydrofracture due to fluids escaping the slab. Similar transient processes may have affected terrane accretion in the geologic past.

Plain Language Summary Some oceanic plates carry large pieces of buoyant, thick oceanic crust or fragments of continental crust. If these pieces are large enough to resist being pulled down during subduction, they stick to the edge of continents and are called terranes. A terrane stuck beneath the edge of a continent may cool the deeper parts of the subduction zone. We show that this has happened in the Cauca region of Colombia. Part of the thick oceanic crust that forms Panamá and the northwestern edge of Colombia has been trapped beneath South America to 125 km depth. It has cooled the area, allowing brittle fractures—earthquakes—to occur above the subducting oceanic plate. This makes the region different from all other subduction zones where earthquakes below 70 km depth occur only in subducting oceanic plates. Cauca earthquakes are mostly above the location the subducted oceanic plate has the most earthquakes. We suspect that water released by the oceanic plate is helping to cause earthquakes above the plate. Future tests will see if water is important here or if the terrane is being warmed by the deep parts of the subduction zone, causing the earthquakes. Other terranes likely acted similarly in the geologic past.

1. Introduction

Terrane collision is a critical process in the evolution of many subduction zones and orogenic systems (e.g., Himalaya-Tibet: Yin & Harrison, 2000; Kapp & DeCelles, 2019; Western North America: Dickinson, 2009; Wells et al., 2014; Ecuador-Colombia: Restrepo & Toussaint, 2020; Toussaint & Restrepo, 2020; Jaillard, 2022; Mediterranean: Dilek & Sandvol, 2009; Robertson et al., 2012). The ultimate fate of a terrane is typically conceptualized as ranging from complete subduction to underplating beneath the overriding plate to direct frontal accretion (e.g., Tao et al., 2020; Tetreault & Buiter, 2012, 2014; Vogt & Gerya, 2014). The accretion of island arc and oceanic plateau terranes onto continental margins plays an important role in the long-term growth of continental crust (Stern & Scholl, 2010). However, understanding of the processes that accompany terrane accretion,

Writing – review & editing: Linda M. Warren, Pablo Aravena, Sungwon Cho, Lillian Soto-Cordero, Patricia Pedraza, Germán A. Prieto, Viviana Dionicio

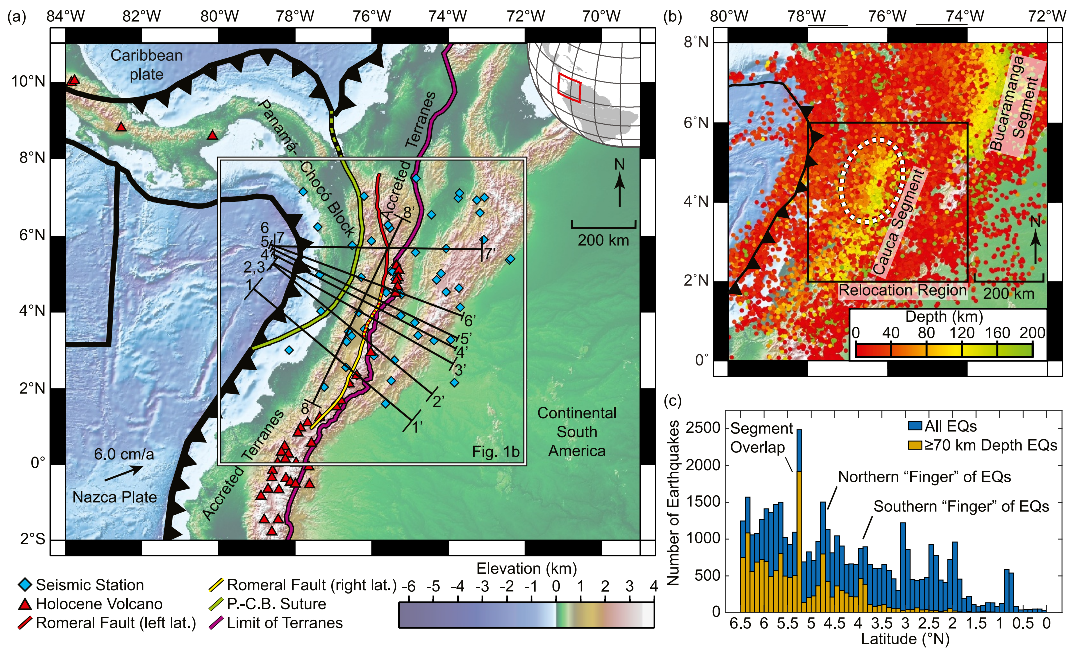

Figure 1. (a) Map of northwestern South America and southernmost Central America showing major tectonic features of the region, seismic stations used in this study, and location of cross-sections shown in Figures 2–5 with corresponding swath widths. Holocene volcanic centers are from Global Volcanism Program (2024). Romeral Fault is modified from Taboada et al. (2000) and Ego et al. (1995). Panamá–Chocó Block (P.-C.B.) suture is compiled from León et al. (2018) and Lara et al. (2018). Other boundaries of the Panamá–Chocó Block compiled from Carvajal-Arenas and Mann (2018) and Linkimer et al. (2010). Limit of accreted terranes is compiled from Cochrane et al. (2014) and Mora-Bohórquez et al. (2017). Topography data from Ryan et al. (2009). (b) All reported RSNC 2010 to July 2019 hypocenter locations (Servicio Geológico Colombiano, 1993b) plotted so that deeper earthquakes overlie shallower ones. The subset relocated in this study is marked by the black box. Bucaramanga and Cauca segments from Pennington (1981). White ellipse marks the approximate extent of the Cauca cluster within the Cauca segment. Note that the offset of the two segments is interpreted to be the Caldas Tear (Vargas & Mann, 2013) though it may instead represent the southernmost edge of the Caribbean plate's subducted lithosphere (e.g., Kellogg et al., 2019). (c) Histogram of all reported RSNC 2010 to July 2019 hypocenters plotted by latitude. The segment overlap marks location of the small area of overlap between the Bucaramanga and Cauca segments seen in (b) and of the proposed location of the Caldas Tear, northern and southern elongate, slab-normal fingers of seismicity mark location of supraslab, intermediate depth (≥70 km) seismicity observed by Chang et al. (2017). Note that intermediate depth seismicity is nearly non-existent south of 2°N, the southern boundary of our relocated subset of earthquakes.

especially those processes occurring at mantle depths, has been largely limited to inferences drawn from material exhumed following continental collision (e.g., Agard, 2021; Angiboust & Raimondo, 2022; Hacker et al., 2013). Observation of these processes in situ requires the identification of locations where terrane accretion and active subduction are ongoing. Here we show that the unusual intermediate depth seismicity observed above a subducting slab in Colombia's Cauca region (Chang et al., 2017, 2019) represents such an in situ process associated with the ongoing accretion of the Panamá–Chocó Block to northwest South America (Figure 1a).

Subduction zone earthquakes typically occur within one of three settings. Shallow earthquakes with hypocenter depths of <70 km (see discussion in Frohlich, 2006) occur along the subduction interface (e.g., Bilek & Lay, 2018) or within the overriding plate's crust (e.g., Madella & Ehlers, 2021; Sippl et al., 2018) and infrequently in its mantle (e.g., Bie et al., 2020; Halpaap et al., 2019; Laigle et al., 2013). At greater depths, the majority of earthquakes occur within the Wadati–Benioff zone, one or two dipping bands of earthquakes that occur within the subducting oceanic plate (e.g., Brudzinski et al., 2007; Florez & Prieto, 2019). The Cauca region in Colombia (the Pacific coast and cordillera west of ~75°W and south of ~5.5°N) represents the only documented location where intermediate (70–300 km) depth seismicity has occurred, continuously for multiple decades, within the mantle wedge above rather than only within a subducting oceanic plate (Chang et al., 2017, 2019). In this study, we relocate seismicity from 2010 to 2019 reported by the Servicio Geológico Colombiano (SGC, Colombian Geological Survey) occurring below 10 km depth in the Cauca region to show that Cauca seismicity largely frames and occurs within a deeply subducted portion of the accreting Panamá–Chocó Block. We then discuss the implications this tectonic context has for the physical mechanism responsible for Cauca seismicity and plate tectonic processes.

1.1. Evolution of the Western Colombian Active Margin

Terrane accretion has dominated western Colombia throughout the Phanerozoic, though the precise timing and even the number of constituent terranes remains contentious (see reviews and efforts at regional reconciliation in Restrepo and Toussaint (2020), Toussaint and Restrepo (2020), and Cediel & Shaw (2019)). These terranes incorporate both continental and oceanic affinity materials exposed in the Central Cordillera and components of the Caribbean oceanic lithosphere (COL, including both the Caribbean Large Igneous Province and island arc material) which make up the basement of the Western Cordillera and modern forearc (Figure 1a). Cauca segment (Pennington, 1981) seismicity generally occurs beneath COL derived terranes (see Figure 1b), and as we argue below specifically in association with the Panamá–Chocó Block, suggesting a possible relationship between this seismicity and the history of these COL derived terranes.

Initial collision of the leading edge of the COL with northern South America likely occurred ∼100–80 Ma progressively from the south to the north with a significant strike-slip component (e.g., Boschman et al., 2014; Braszus et al., 2021; Montes et al., 2019; Pindell & Kennan, 2009; Pindell et al., 2005). Plate reconstructions constrained by tomographic slab models (Braszus et al., 2021) and the development of arc volcanism within both the pre-collisional South American margin (Cardona et al., 2020; Jaramillo et al., 2017; Leal-Mejía et al., 2019; Zapata et al., 2019) and northeastern edge of the Caribbean plate (Jaramillo et al., 2017; Leal-Mejía et al., 2019; Pindell & Kennan, 2009; Zapata et al., 2019) require subduction of the intervening Proto-Caribbean oceanic lithosphere both eastward beneath South America and westward beneath the Caribbean. After collision with the leading edge of the Caribbean plate, subduction reinitialized beneath the northwest South American margin (Jaramillo et al., 2017; Pindell et al., 2005; Zapata et al., 2019) as part of a trench-trench-trench triple junction between the South American, Caribbean, and Farallon plates (e.g., Pindell et al., 2005; Boschman et al., 2014; Barbosa-Espitia et al., 2019 Montes et al., 2019, González et al., 2023; though see e.g. Leal-Mejía et al., 2019 for alternative interpretation).

The trench-trench-trench triple junction eventually brought components of the intra-oceanic Panamá–Chocó volcanic arc on the southwestern margin of the Caribbean plate into contact with the Colombian Trench. The earliest evidence for significant interaction of these may be indicated by the beginning of deformation recorded in the Panamá portion of the arc at ∼38–40 Ma (Barat et al., 2014; Buchs et al., 2019; Montes et al., 2012), approximately contemporaneous with the 45–39 Ma shutdown of arc volcanism in the South American plate north of the triple junction (Barbosa-Espitia et al., 2019; Cardona et al., 2018). Subduction of the Caribbean Plate around the triple junction continued at a rate of ∼20 mm/yr until 28–20 Ma when the Chocó portion of the arc presently exposed at the surface made contact with South America (Ariza-Acero et al., 2022; González et al., 2023; Montes et al., 2012), requiring that between 220 and 380 km of the Panamá–Chocó arc was subducted prior to its accretion as the Panamá–Chocó Block, the western-most COL terrane, in the late Oligocene or early Miocene (e.g., Ariza-Acero et al., 2022; Lara et al., 2018; Montes et al., 2012; Piedrahita et al., 2017; Suter et al., 2008). Geodetic observations show that the Panamá portion of the block north of ∼7°N acts as an eastward-moving indenter (Jarrin et al., 2023; Kellogg et al., 2019), while the southern Chocó portion of the block moves with adjacent parts of the Colombian Andes (Jarrin et al., 2023; Kellogg et al., 2019) indicating that accretion is an ongoing process. This is also reflected in a change in regional faulting near the southeastern edge of the Chocó portion between 3°N and 4.5°N (Figure 1a) where the Romeral strike-slip fault switches from left-lateral to right-lateral/transpressional (Ego et al., 1995; Jarrin et al., 2023; Taboada et al., 2000) and more minor Quaternary faults mark an active right-lateral shear zone cross-cutting the Romeral fault (Suter et al., 2008). These features likely represent the final stages of suturing of the southern portion of the block to the South America plate which began with the reestablishment of arc volcanism to the northwest of the presently active arc at ∼12 Ma (Rodríguez & Zapata, 2012; Zapata-García & Rodríguez-García, 2020; Weber et al., 2020; and review in Marín-Cerón et al., 2019). Little volcanism postdating the block's accretion has been reported within the modern volcanic arc gap between 3.5°N and 5°N (Marín-Cerón et al., 2019), suggesting the present gap is a persistent feature.

Below, we show that the majority of intermediate depth, supraslab (lying above the Nazca slab as defined by the slab's planar Wadati–Benioff zone) seismicity in the Cauca segment occurs in association with a previously unknown ∼180 km long segment of the Panamá–Chocó Block thrust beneath the Colombian Western Cordillera.

The top of this feature is a dipping plane of seismicity, clearly separable from the Wadati–Benioff Zone of the Nazca plate, running from ∼10 km depth at the mapped suture between ∼3.5°N and ∼4.5°N to ∼75 km depth at ∼3°N. This approximately coincides with the switch in left-lateral to right-lateral slip in the Romeral Fault noted above. Intense supraslab seismicity down to ∼125 km depth may mark the downdip termination of the subducted block, near the approximate center of the gap in the volcanic arc. More diffuse supraslab seismicity characterizes the region above the subducted portion of the block, within either the original lithospheric mantle of the earlier accreting terranes or trapped, frozen mantle wedge asthenosphere between the block and overlying terranes. North of ∼5.5°N intermediate depth seismicity disappears, inhibiting detailed analysis through earthquake relocation and perhaps indicating a significant structural change to the north of the paleo-triple junction.

1.2. The Cauca Cluster: Long-Term, Deep Seismicity Beyond a Subducting Plate

The Cauca cluster occurs within the region between 3.5°N to 5.5°N and 75.3°W to 77°W (Chang et al., 2017; Cortés & Angelier, 2005), encompassing roughly the northern half of the Cauca segment between ∼1.5°N to 5.5°N and 75°W to 77°W (Cortés & Angelier, 2005; Pennington, 1981). While comprising ∼17% of the Cauca segment's area, the cluster accounts for ∼68% (258 of 380) of intermediate (70–300 km) depth seismicity reported for the segment in the International Seismological Centre's global earthquake catalog for 1964 to 2022 with magnitudes >4.0 (International Seismological Center, 2024). Regional earthquake detections from the SGC's network show a more pronounced dominance of the Cauca cluster over Cauca segment seismicity for the 2010 to mid-2019 period: 45% (9,235 of 20,744) of all recorded events and 83% (4,809 of 5,769) of all events between 70 and 300 km depth occurred in the cluster (Servicio Geológico Colombiano, 1993b; see also Figures 1b and 1c). Within the cluster, a pair of structures were previously observed to extend ∼30–40 km orthogonally from the well-defined dipping plane of Wadati–Benioff zone seismicity in the Nazca Plate (Chang et al., 2017; see locations in Figure 1c) and previously misidentified as part of the slab (e.g., Cortés & Angelier, 2005; Ojeda & Havskov, 2001; Pennington, 1981). Supraslab earthquakes within these structures are evident in the catalog extending back to 1964 examined by Pennington (1981) and continue through the present, making the Cauca cluster the most persistent documented example of intermediate depth supraslab seismicity, lasting well beyond the <1 year-long sequences reported elsewhere (e.g., Špičák et al., 2004, 2009; White et al., 2019) and laying ∼50–100 km deeper than other shallow, long-lasting examples of mantle wedge seismicity from subduction zones (e.g., Bie et al., 2020; Davey & Ristau, 2011; Halpaap et al., 2019; Laigle et al., 2013; Nakajima & Uchida, 2018; Nakata et al., 2019; Paulatto et al., 2017; Uchida et al., 2010) with much higher thermal parameters (Syracuse et al., 2010), which would (contra Halpaap et al., 2021) be expected to indicate a significantly warmer subduction zone in Colombia than at these other locations.

We suggest that the subducted continuation of the Panamá–Chocó block is directly responsible for the existence of the Cauca cluster. This block of lithosphere appears to lie directly above the top of the slab from the megathrust down to ∼125–150 km depth at its greatest extent, enabling seismogenic processes usually associated with subducting slabs to occur within a block of cold, supraslab material. The stationarity of the material containing the Cauca cluster provides a unique chance to evaluate proposed causes of intermediate depth seismicity. Numerical modeling of subduction zones has shown that a steady state thermal structure is achieved on ∼12 Myr timescales (van Keken et al., 2018), indicating that the material hosting the Cauca cluster should have a near steady-state thermal structure given the date of its subduction and the continuous refrigeration caused along its base by the subducting slab. This greatly reduces the effects of progressive mineral phase changes that complicate interpretation of slab seismicity. We conclude by exploring the implications our observations have for different proposed causes of slab seismicity as a basis for future work on this long-standing problem in subduction zone science.

2. Method

Double-difference earthquake relocation approaches (e.g., Waldhauser & Ellsworth, 2000; Waldhauser & Schaff, 2007) attempt to reduce or eliminate the effect of unknown three-dimensional variations in seismic velocity between earthquake sources and seismic stations on calculated earthquake hypocenter locations. Pairs of earthquakes separated by arbitrarily short distances are assumed to follow near-identical ray paths to a seismic station and be affected equally by velocity variations encountered along the path. Differences in arrival times, with origin time removed, between pairs of neighboring events can be attributed to their spatial separation. By incorporating a minimum of eight observations of an earthquake pair (providing four differential measurements for each earthquake in the pair), this separation can be defined in three spatial dimensions and in time. Incorporation of additional stations observing each event pair, of additional earthquakes to pair with, and of both P- and S-phase arrival information can improve precision of earthquake hypocenter locations (Waldhauser, 2001; Waldhauser & Ellsworth, 2000). For neighboring earthquakes with broadly similar waveforms, further precision may be obtained by using arrival cross-correlation to reduce uncertainties inherent to manual phase arrival picking.

Earthquake locations provided by double difference approaches are robust only in a relative sense. As we have previously shown with a more computationally tractable, non-cross-correlated data set (Bishop et al., 2023) the absolute locations of hypocenters are highly variable depending on the assumed regional velocity model, P-wave velocity to S-wave velocity ratio (Vp/Vs ratio), and systematic offsets in initial catalog earthquake location, but the overall configuration of hypocenters varies in only minor detail. An exception to this occurs for events immediately above and below a strong, horizontal velocity contrast like the Mohorovičić discontinuity that is not exactly matched by the velocity model due to differences between true and modeled ray paths. If the contrast is modeled shallower than its true depth, hypocenters near the boundary will tend to be pushed away from the modeled contrast; if the modeled contrast is deeper, hypocenters will tend to be pulled toward the modeled contrast (Bishop et al., 2023). Hypocenter configuration does not change significantly with error in event origin time of at least 2 s and arrival time error of up to 0.5 s (Bishop et al., 2023), approximately equivalent to the average picking error of 0.43 s for seismic network analysts for events at local distances and low signal-to-noise (Zeiler & Velasco, 2009).

We have used the double-difference method implemented in HypoDD (Waldhauser, 2001; Waldhauser & Ellsworth, 2000) to relocate hypocenters based on locations and P- and S-arrival times reported in the SGC catalog. This approach was previously used for a subset of our data set by Chang et al. (2017) and our goal is to build on this work over a larger region and longer duration while providing hypocenter uncertainty estimates for seismicity in the region, a computationally intensive problem not attempted at this scale by Chang et al. (2017). We used the single-value decomposition approach implemented in HypoDD to obtain mathematically valid estimates of hypocenter uncertainty (Waldhauser, 2001; Waldhauser & Ellsworth, 2000), despite the high computational costs (see Section 3 below). We have run our relocation for a much larger $4° \times 4°$ region than prior studies of the Cauca cluster to both investigate the regional context of the cluster and reduce the possible effects of systematic offset in initial hypocenter location. We further used the optimal regional 1-D P-wave velocity model and Vp/Vs ratio obtained by Ojeda and Havskov (2001) for central Colombia as this model and ratio are used to locate the majority (>95%) of events in the RSNC catalog. Incorporation of a regionally accurate Vp/Vs ratio and S-wave arrival information provides constraints previously shown to improve both the ability to locate shallow hypocenters and overall hypocenter location accuracy relative to P-wave information alone (e.g., Chiu et al., 1997; Gomberg et al., 1990). However, the lack of a 3D velocity model for the region will cause subsets of hypocenters to be systematically shifted due to the presence of strong lateral velocity gradients (e.g., comparison of 1D and 3D locations in Zhang & Thurber, 2003).

3. Data

We have used 10 years of phase-pick arrival times and hypocenter initial locations from the RSNC catalog (Servicio Geológico Colombiano, 1993b; http://bdrsnc.sgc.gov.co/paginas1/catalogo/index.php) from 1 January 2010 to 5 July 2019 for the $4° \times 4°$ region centered on the Cauca cluster and running from 2°N to 6°N and 74°W to 78°W (see black box in Figure 1b). More than 95% of hypocenter locations in the RSNC catalog during our study period were obtained use the regional velocity model from Ojeda and Havskov (2001), while remaining hypocenters were obtained using a variety of local velocity models (e.g., Londoño et al., 2019; Pedraza & Pulido, 2018; Poveda et al., 2018). We have not utilized cross-correlation picks as prior investigation of supraslab seismicity in the region has shown that focal mechanisms of these earthquakes are too variable to yield reliable cross-correlation picks (Chang et al., 2017). We use the full range of magnitudes reported by the SGC for our study area, from nominal 0.5 M_l to 6.1 M_W. We selected events with reported hypocenter depths of ≥10 km to minimize the number of relocations that have negative depth (so called "airquakes," see Waldhauser, 2001) and at least three stations within 450 km of the epicenter. We then assigned weighting factors to P- and S-phase arrivals based on station-epicenter distance: distances of less than 100 km were assigned a weight of 0.9, 100–150 km were assigned 0.8, 150–200 km were assigned 0.7, and 200–450 km were assigned 0.5. Computational limitations and the SGC's shift from SEISAN to SeisComp3 hypocenter determination at the end of February 2018 required us to

10.1029/2024JB030067

divide our data set into 8 segments run as independent inversions in HypoDD. 1 January 2010 to 28 February 2018 were divided into seven 14-month long segments while the final segment covered 23 February 2018 to 5 July 2019 (see Supporting Information S1 regarding overlap of the final two segments), ∼16 months. The final segment required 54 days of computation time to relocate an initial set of 3,196 events compared to the 2 days required by the seventh segment to relocate an initial set of 1,566 events, reflecting both an improvement in the SGC's ability to detect events and how doubling the number of events inverted by HypoDD exponentially increases computation time.

HypoDD places a number of internal data quality requirements on pairs of events prior to inversion. We required that all event pairs and stations used in the inversion be separated by at most 200 km. This resulted in a total of 61 usable stations (Figure 1 and Table S1). Hypocenters in each event pair were further required to lie within 50 km of each other, have a minimum of 10 and maximum of 50 observations for each event pair, have a minimum of 8 observations to define a neighboring event, and have a maximum number of 10 neighboring events. While most of these values are restrictive and should help to ensure stable solutions, we greatly relaxed the maximum distance between hypocenters in a pair (typically ∼15–20 km for subduction zone settings, see double-difference used by e.g. Rietbrock & Waldhauser, 2004; Zhang et al., 2004; Chang et al., 2017; Linkimer et al., 2020) as a way to assess the appropriateness of typical a priori values used for this parameter. The weighted average of the distance between hypocenters in a pair for our entire data set is 15.1 km, indicating that the event pairs satisfying other quality requirements are largely contained within an appropriate range of separation without imposing a strongly restrictive a priori constraint.

Taken together, these selection criteria resulted in a total of 8,306 events suitable for relocation with 171,812 P-phase differential times and 166,951 S-phase differential times. Of these, 1,017 events were isolated and unsuitable for HypoDD relocation, leaving 7,289 candidates for relocation.

4. Results

A total of 6,722 earthquakes out of the 7,289 relocation candidates were relocatable using HypoDD, representing a successful relocation rate of 92%. A full catalog of our relocations is provided in Table S2 and a more detailed examination of event uncertainties is provided in Supporting Information S1. As shown in Figure S1, vertical and lateral uncertainties of the relocations are not normally distributed and 67% of relocations have all directional uncertainties <5 km compared to only 42% of the input catalog locations. 1σ standard deviations for latitudinal, longitudinal, and depth uncertainties are 11.9 km, 21.8 km, and 16.3 km. These values approximate the scale of the smallest features we examine, and as such we plot or interpret only the 6,375 hypocenters with smaller spatial uncertainties. No strong correlation exists between relocation uncertainty and hypocenter origin time (Figures S2a and S2c in Supporting Information S1)—indicating uncertainties are largely unaffected by changes to the network over our study period or by our division of the data set into time intervals. Relocation uncertainties' relationship to the relocated hypocenters' spatial position can be most easily examined in terms of distance from the relocated hypocenters' centroid. No strong correlation exists between relocation uncertainty and distance from the relocated hypocenters' centroid for events within 2.82° (the maximum distance from the center of our study region to its corners; Figures S2b and S2d in Supporting Information S1) of the centroid (6,716 hypocenters).

4.1. Defining the Cauca Cluster's Structures Through Earthquake Locations

Figures 2 and 3 provide cross-sections showing our relocations and their uncertainties along trench ∼perpendicular (Figures 2 and 3a–3c) and trench ∼parallel (Figure 3d) orientations (compare with initial catalog location uncertainties in Figures S3 and S4 in Supporting Information S1). Swath width for each cross-section varies in order to capture structures of interest or to illustrate separation between these structures. A number of structures cross discontinuities within the velocity model used to calculate our relocations. As noted above in Section 2, this may produce artifacts within ∼2–3 km of the discontinuity. To check for these effects, we have plotted the velocity model's discontinuities on each cross-section in red (≥1 km/s difference across the discontinuity), yellow, (0.4 km/s difference), or green (0.1 km/s difference). Figures 2 and 3 show little effect on the density of events about these discontinuities and the depth histogram in Figure S5 in Supporting Information S1 shows no departures from large scale trends at these discontinuities at our depths of interest, collectively indicating these discontinuities have little effect on the structures seen in our relocations. Structural complexity

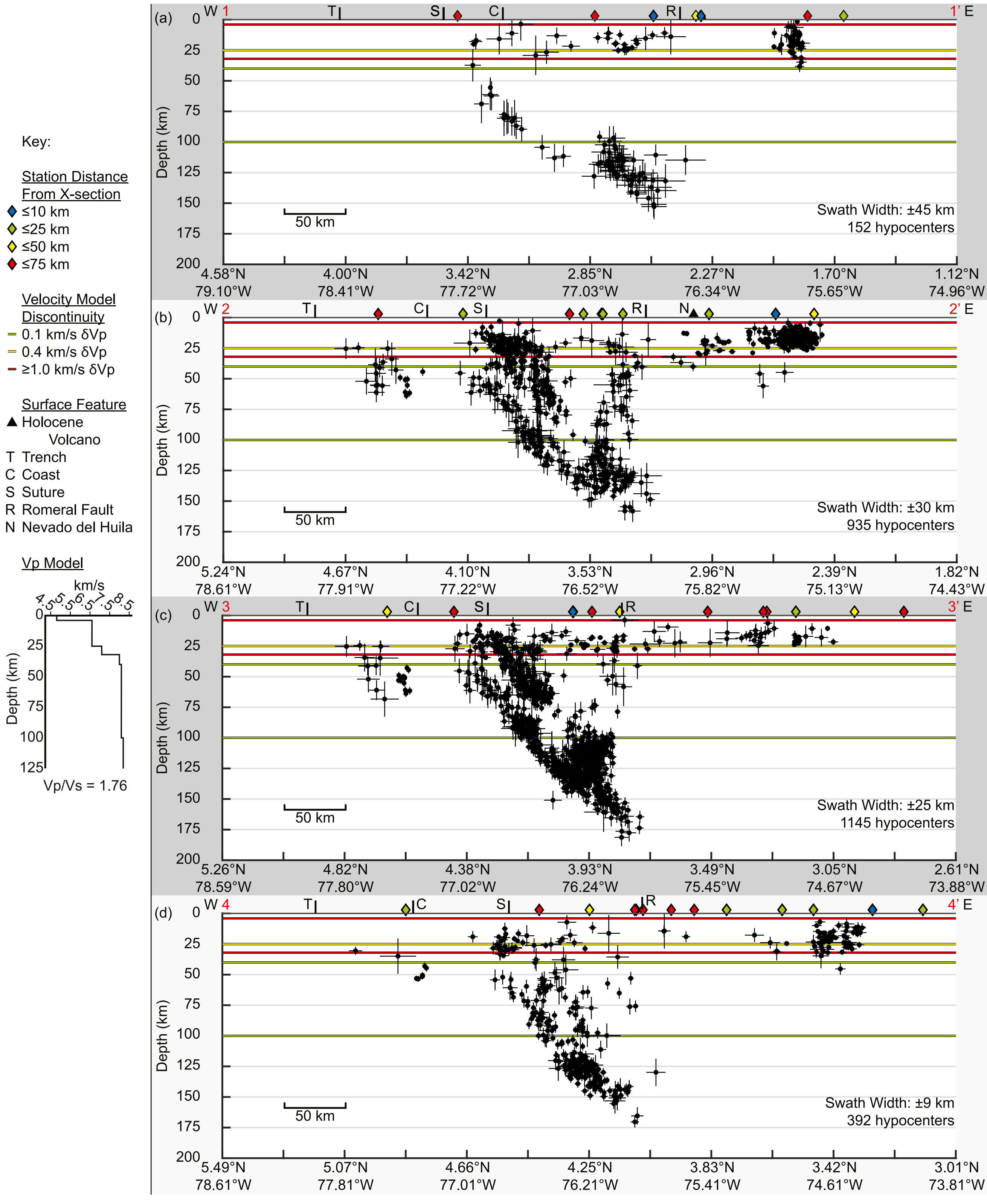

Figure 2. Cross-sections 1-4 (see Figure 1 for locations) showing relocation results (black dots) and their 2σ uncertainties. Red numbers mark ends of lines. Horizontal colored lines mark depths of changes in velocity in 1-D model used for relocation, shown at left (from Ojeda & Havskov, 2001). Trench (T), Coast (C), Panamá–Chocó Block suture (S), and Romeral Fault (R) provided to aid in orientation. See text for discussion.

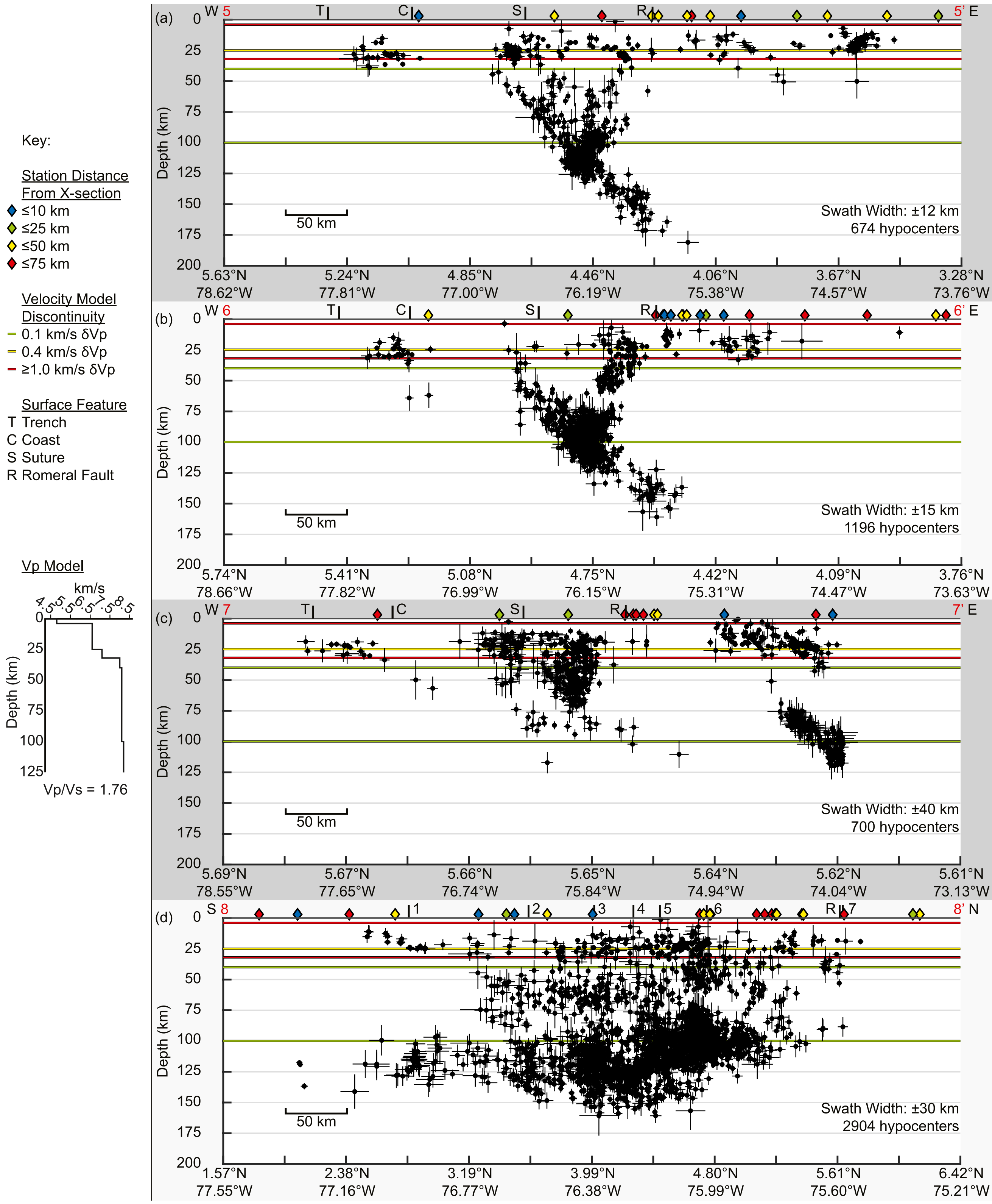

Figure 3. Cross-sections 5-8 (see Figure 1 for locations) showing relocation results (black dots) and their 2σ uncertainties. Black numbers 1–7 in panel (d) mark intersection of cross-section 8-8' with other cross-sections. All other features as in Figure 2. See text for discussion.

increases from south to north in our study region, and as such we examine the cross-sections beginning with the southernmost.

Cross-section 1-1’ (Figure 2a) passes through the region south of the Cauca cluster. Earthquakes in this region are comparatively infrequent and easily divisible into three groups: a dipping feature resolvable from ∼50 to ∼150 km depth west of the volcanic arc, scattered events above this dipping feature limited to <25 km depth, and a more compact set of events east of the volcanic arc which may extend slightly deeper to ∼30 km depth.

Cross-section 2-2’ (Figure 2b) passes through the southern edge of the Cauca cluster, highlighting the greater productivity of the cluster. Clear groupings within the earthquakes are more difficult to distinguish than along 1-1’, however the hypocenters can be divided into several features. Between 77.9°W and 77.5°W, a small number of events between ∼25 and ∼60 km depth are clearly separable from other features. The large wedge-shaped group west of the volcanic arc between 77.2°W and 76.1°W can be subdivided into three features: a lower dipping feature from ∼50 to >150 km depth, a shallower dipping feature from <10 to ∼80 km depth, and a residual subset of events above and to the east of these dipping features with little internal structure. We see no evidence for the elongate, slab-normal fingers of seismicity at 75 and 105 km depth previously interpreted in this area (Martínez-Jaramillo & Prieto, 2024). We suggest that by dividing their data set into two groups relocated separately above and below 60 km depth, Martínez-Jaramillo and Prieto (2024) may have inadvertently separated the shallow dipping feature we image into these fingers. In contrast, our residual subset of events does offer a clear match for the deepest finger of supraslab seismicity reported by Martínez-Jaramillo and Prieto (2024) beginning at ∼135 km depth and extending to crustal depths. Differing from the suggestion of Martínez-Jaramillo and Prieto (2024), our results show that this feature is unlikely to be a direct fluid pathway between the slab and the volcanic center Nevado del Huila as it lies ∼50 km west of the center. The events closer to Nevado del Huila can be largely associated with a period of intense volcanic unrest in January 2019 and likely represents a deeper continuation of the <10 km depth seismicity reported by the Observatorio Vulcanológico y Sismológico de Popayán (Sevicio Geológico Colombiano, 2019a, 2019b). Finally, east of the volcanic arc, we once again distinguish a compact group of events down to ∼30 km depth.

Cross-section 3-3’ (Figure 2c) passes both through a gap in the active volcanic arc and through the southern finger of seismicity that extends ∼perpendicular to the slab identified by Chang et al. (2017). Clear groupings become more distinguishable within the distribution of earthquakes along this cross-section. A small number of events between 77.8°W and 77.4°W between ∼25 and ∼60 km depth are again clearly separable from the others along this section. East of these, three features dominate: a continuation of the lower dipping feature, this time stretching from ∼50 to ∼175 km depth; a shallower dipping feature from <10 to ∼70 km depth; and a mass of seismicity from ∼100 to ∼125 km depth centered near 76.2°W. This third feature spatially corresponds to Chang et al. (2017)'s southern finger of seismicity. While recent receiver function results for the region from Mojica Boada et al. (2022) do not have sufficient lateral resolution to image possible changes in the velocity structure around the shallow dipping feature or finger of seismicity, these two groups of seismicity are limited to the region where receiver functions detect little velocity contrast between the continental crust and underlying forearc mantle. This suggests the mantle containing the seismicity may have an unusual composition. Additional shallow seismicity is largely limited to <25 km depth.

Cross-section 4-4’ (Figure 2d) lies within the gap in the volcanic arc and within the ∼20 km space separating the mass of seismicity at 76.2°W on cross-section 3-3’ from a similar feature to the north on cross-section 5-5’. A small number of earthquakes occur well west of the others between 77.8°W and ∼77.4°W between 25 and 50 km depth. The equivalent to the lower dipping feature on cross-sections 1-1’ to 3-3’ appears here from ∼50 km depth to ∼150 km depth, however the upper dipping plane (if present) appears to have been reduced to two patches of moderately concentrated seismicity at ∼25 and ∼60 km depth. Shallow seismicity is dominated by a compact group of earthquakes near 74.6°W at less than ∼30 km depth.

Cross-section 5-5’ (Figure 3a) lies north of the gap in the active volcanic arc and passes through a second mass of seismicity stretching ∼perpendicular to the subducting slab. A distinct group of shallow earthquakes between ∼25 and ∼30 km depth at 77.8°W to 77.4°W lies well west of other events. Two features are prominent in the central part of the cross-section: a dipping plane running from ∼50 to ∼175 km depth and a mass of seismicity ∼perpendicular to this plane centered near 76.2°W between ∼90 and ∼110 km depth. Scattered seismicity may run from the top of this mass of seismicity to ∼50 km depth. Shallow seismicity occurs above ∼30 km depth and is concentrated in two locations, one near 76.6°W and one east of ∼74.5°W.

Cross-section 6-6' (Figure 3b) passes through the active volcanic arc and through the northern finger of seismicity identified by Chang et al. (2017). The isolated group of events at <30 km depth between 77.8°W and 77.4°W lies well removed from other features. The most intense seismicity along the cross-section lies within a dipping plane of events from ~50 to ~150 km depth and a mass of seismicity centered at ~76.1°W between 75 and 100 km depth and ~perpendicular to the dipping plane. This mass of seismicity spatially corresponds to Chang et al. (2017)'s northern finger of seismicity. A less concentrated group of events appears to extend from this mass to a depth of ~25 km, however a gap of ~25 km between these two features complicates interpretation of any possible relationship between them. Shallow seismicity is infrequent and largely limited to <25 km depth.

Cross-section 7-7' (Figure 3c) runs parallel to the hypothesized Caldas Tear/southern edge of the subducted Caribbean plate (hereafter referred to as the Caldas Tear for brevity; see Figure 1a; Vargas & Mann, 2013; Kellogg et al., 2019), which separates the Cauca and Bucaramanga slab segments. The events between 78.1°W and ~77.5°W at <30 km depth may have a weakly developed continuation at ~60 km depth near 77.2°W, however these events are isolated from other features. A dense, wedge-like group of seismicity occurs from <10 to ~75 km depth between 76.7°W and 75.8°W while a possible, weakly developed plane lies below this feature at ~75 to >100 km depth. An intense, dipping band of seismicity between 75 and ~125 km depth from ~74.5°W to ~74.0°W is spatially coincident with the southern edge of the Bucaramanga segment (e.g., Prieto et al., 2012; Syracuse et al., 2016). This seismicity associated with the Bucaramanga segment is well separated (>50 km) from seismicity occurring within the Cauca segment at similar depths, suggesting little if any direct interaction between the two seismically active zones. Shallow seismicity above the Bucaramanga segment appears largely limited to <30 km depth and does not extend west of the volcanic arc, making it easily distinguishable from shallow seismicity above the Cauca segment.

Finally, cross-section 8-8' (Figure 3d) provides an approximately trench parallel view stitching together the cross-sections discussed above. This perspective allows for identification of the extent of the Cauca cluster between ~3.2°N and ~5.6°N, the region in which seismicity extends from ~100 to 125 km depth to the surface. The marked intersections between this cross-section and the cross-sections discussed above also allow for the easy identification of the southern (centered near 4°N) and northern (centered near 4.8°N) masses of seismicity above an intense band of seismicity between 4°N and 5.2°N, and somewhat more difficult identification of the central mass of seismicity (centered slightly north of 4.4°N). The lower limit of seismicity along this cross-section also suggests that the planar seismic feature seen in the cross-sections discussed above is moderately undulatory: it deepens somewhat gradually from <100 km at the location of the hypothesized Caldas Tear (Vargas & Mann, 2013; near 5.6°N) to >150 km at the center of the Cauca cluster (~4°N), before shallowing to ~125 km depth south of the cluster near ~2.8°N, near the location of the proposed Malpelo tear (Idarrága-García et al., 2016) and transition to the Ecuador slab segment (Pennington, 1981) influenced by the subducting Carnegie Ridge (e.g., Gutscher et al., 1999).

Cross comparison of the cross-sections presented above as well as additional close examination of hypocenter locations from other orientations allow us to categorize our relocated hypocenters into 11 interpretive groups shown in Figures 4 and 5. The categorization of individual hypocenters near the edges of some groupings, especially where the base of supraslab features approach the Nazca plate's Wadati–Benioff zone, is somewhat ambiguous. We have evaluated these hypocenters on a case-by-case basis to ensure they lie closer to hypocenters that can be unambiguously assigned to a category than to those in neighboring categories. In locations where this is not possible or in locations where classification is otherwise ambiguous, we assign events to a residual category of hypocenters we refer to as "scattered" for brevity. See additional discussion on these events below. Coastal to offshore seismicity (black in Figures 4 and 5) consistently lies well west of other seismicity and at a depth of <30 km (Figures 4b, 4c, 4d and 5a, 5b, 5c); this likely represents seismicity associated with the shallow megathrust while the inboard gap in seismicity may be associated with the locked megathrust. The dipping plane from ~50 km depth to >150 km depth (Figures 4 and 5a, 5b, 5c, dark blue) represents the Nazca slab's Wadati–Benioff zone. In the northernmost part of the study region (Figure 5c), the shallow part of this dipping plane appears to continue to <20 km depth. This shallow continuation is unlikely to represent Wadati–Benioff zone seismicity and instead may represent interactions between the megathrust and forearc structures (see Discussion) or potentially complications related to the Caldas Tear, however distinguishing between these potential features is not possible with the present data set. The three masses of concentrated seismicity ~perpendicular to the Wadati–Benioff zone (Figures 4c and 5a, 5b; dark red, yellow, and green respectively) are, following Chang et al. (2017), interpreted as occurring within the non-convecting mantle wedge corner (see Discussion). The planar feature running from

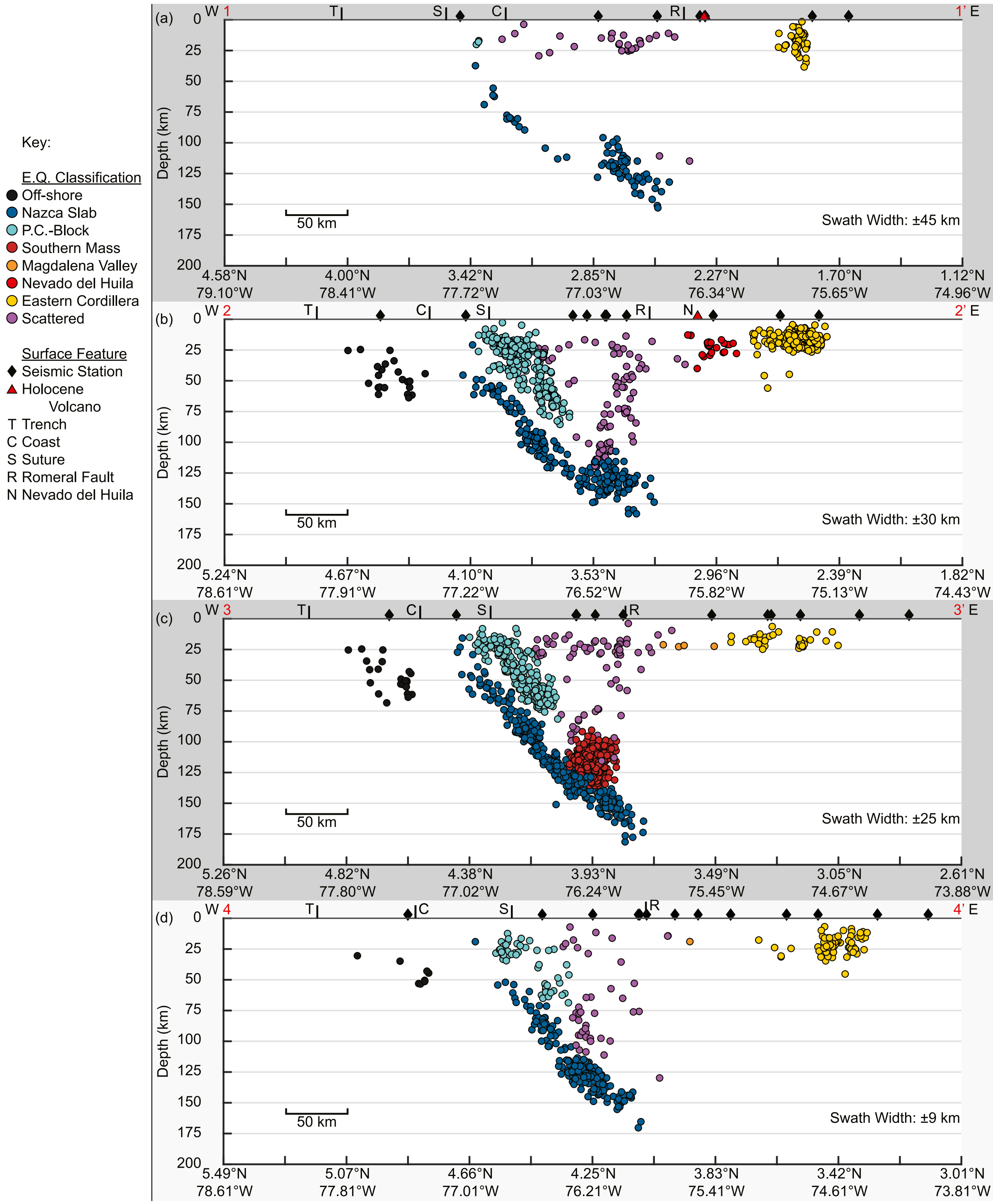

Figure 4. Cross-sections 1-4 (see Figure 1 for locations) showing interpretation of relocated hypocenters. Red numbers mark ends of lines. Colors of hypocenters correspond to different features discussed in the text. Relocated earthquake catalog (see Table S2) includes these classifications. Trench (T), Panamá–Chocó Block suture (S), and Romeral Fault (R) provided to aid in orientation. See text for discussion.

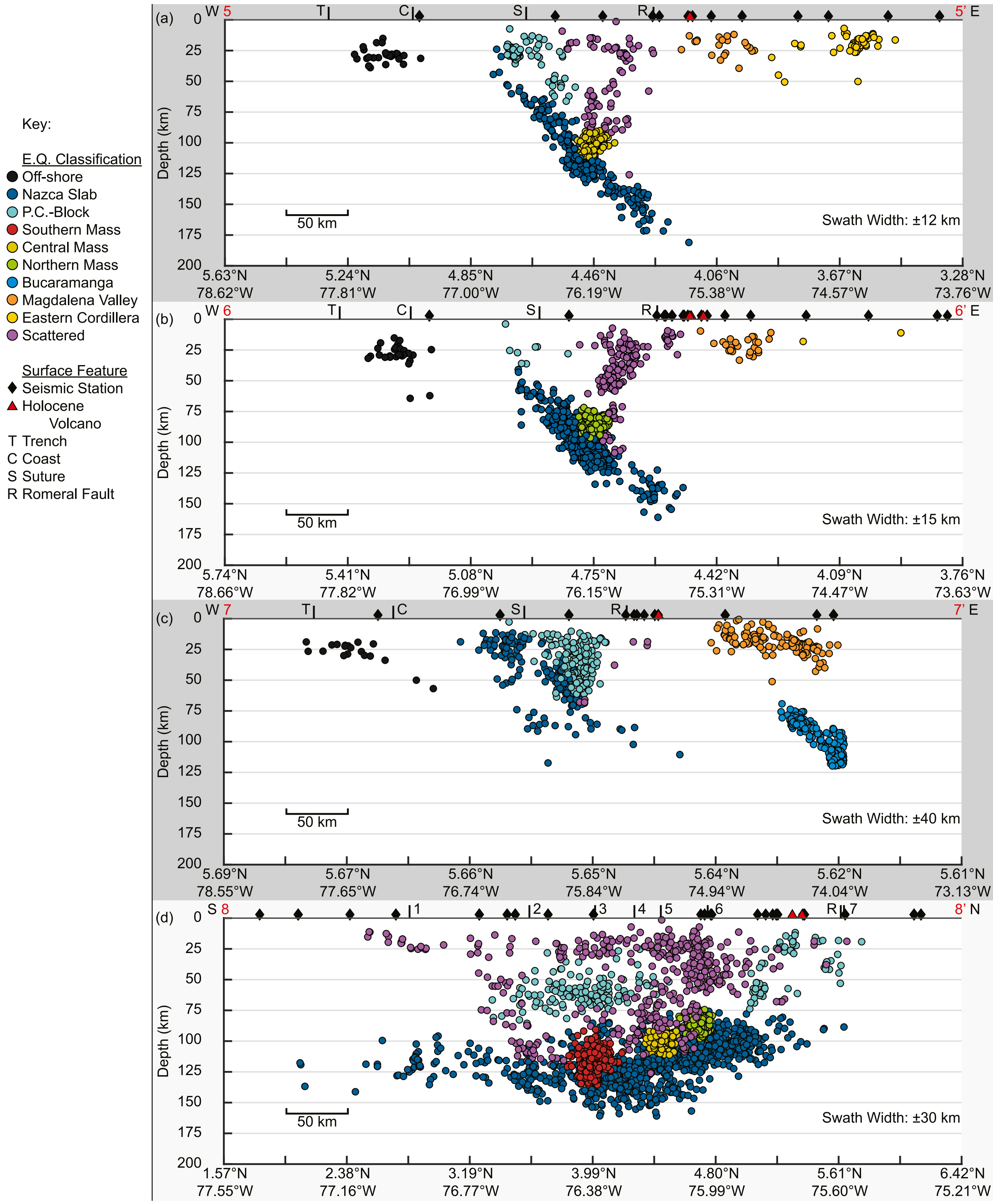

Figure 5. Cross-sections 5-8 (see Figure 1 for locations) showing interpretation of relocated hypocenters. Black numbers 1–7 in panel (d) mark intersection of cross-section 8-8' with other cross-sections. All other features as in Figure 4. See text for discussion.

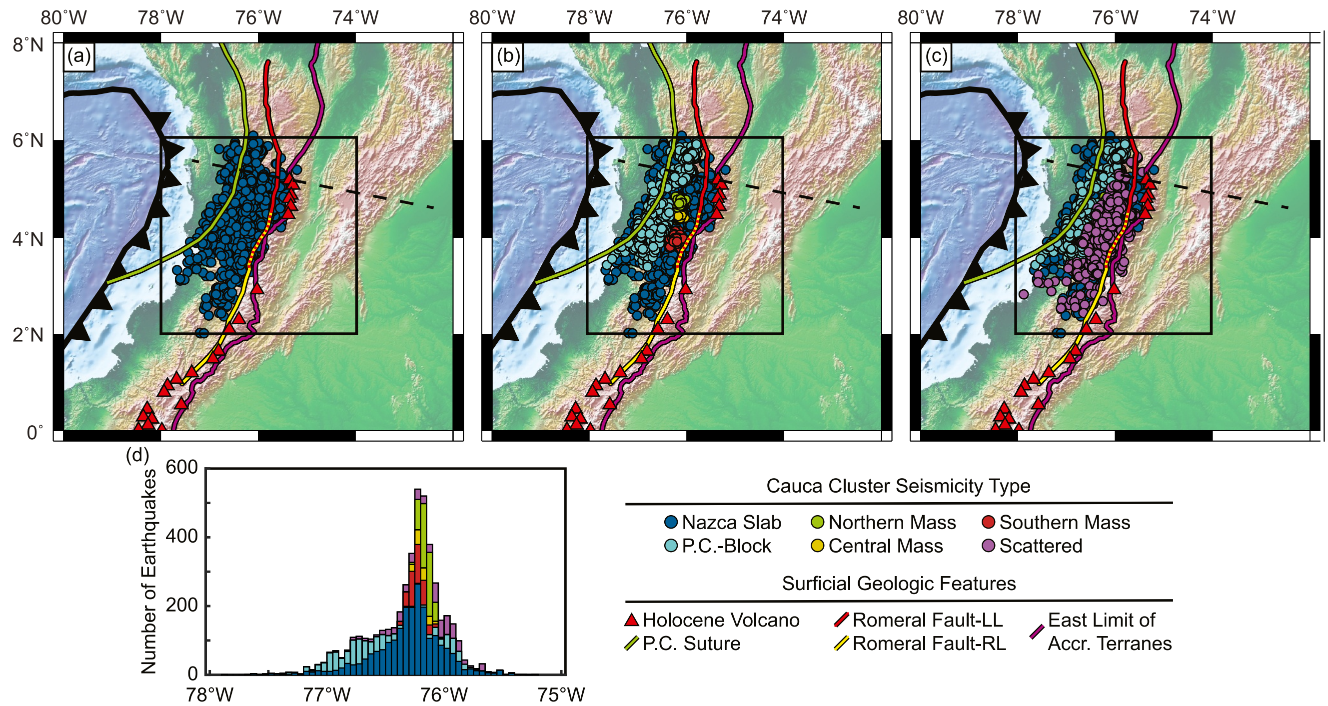

Figure 6. Maps showing association of relocated (a) Nazca slab seismicity, (b) seismicity related to the Panamá–Chocó Block and supraslab masses, and (c) scattered supraslab seismicity to assorted surficial features. Dashed black line marks location of hypothesized Caldas Tear from Vargas and Mann (2013). Note that LL and RL are abbreviations for left-lateral and right-lateral respectively. (d) Histogram showing relocated seismicity associated with the Cauca cluster as a function of longitude. Colors in the histogram correspond to the hypocenter colors in maps in a-c and show the fraction of the corresponding hypocenter types in each bin. Note that the peak in Nazca slab seismicity corresponds to the location of supraslab masses of seismicity and that the Panamá–Chocó block seismicity is clearly divided into two subgroups with the western subgroup related to the southern part of the suture and the eastern subgroup related to the eastern part of the suture. See text for discussion.

~10 km depth near the Panamá–Chocó Block suture to ~80 km depth (see Figures 4b, 4c, 4d, and 5a; cyan), along with a patchier feature located in a similar position relative to the suture in the north (Figure 5c; cyan), are interpreted as representing seismicity driven by continued deformation along the Panamá–Chocó Block suture (see Discussion). Shallow seismicity in the vicinity of the volcano Nevado del Huila (Figure 4b; bright red) can be directly associated with a known episode of volcanic unrest (Sevicio Geológico Colombiano, 2019a, 2019b) while seismicity east of the volcanic arc (Figures 4 and 5a, 5b, 5c; orange and gold) can be divided into two northeast trending features corresponding to transpressional structures within the actively deforming Magdalena Valley (orange) and Eastern Cordillera (gold; e.g. Taboada et al., 2000; Montes et al., 2005; Mora-Páez et al., 2016; Arcila & Muñoz-Martín, 2020). The northern, concentrated plane of seismicity present at the eastern edge of our study area between 75 and 125 km depth (Figure 5c, light blue) is interpreted as Wadati–Benioff zone seismicity within the Bucaramanga segment (Prieto et al., 2012; Syracuse et al., 2016). Remaining seismicity within the Cauca cluster is largely scattered with little discernible structure at crustal to mantle depths. Two exceptions to this occur along cross-sections 2-2' (Figure 4b; purple) and 6-6' (Figure 5b; purple) near the intersections with cross-section 8-8' (Figure 5d). An elongate, near-vertical feature stretches from the Nazca Wadati–Benioff zone to lower crustal depths along 2-2' while a more inclined feature runs from uppermost mantle depths to <20 km depth along 6-6'. These features lie well west of the volcanic arc and seem to terminate at depth near the surface trace of the Romeral Fault.

4.2. Spatial Relationship to Terrane Sutures and Volcanic Arc

The supraslab seismicity in the Cauca cluster is contained entirely within the forearc between the Panamá–Chocó suture and ~25–50 km east of the volcanic arc front (Figure 6). Seismicity within the subducting Nazca plate (Figure 6a) begins well east of the trench and extends to just beneath the active volcanic arc. The slab becomes much less seismically active south of 3°N and seismicity is most intense along a north–south band at 76.25°W (Figure 6d). Panamá–Chocó Block related seismicity tracks the location of the block's suture (Figure 6b) and may be divided into two subgroups: a dipping plane to the southwest (Figures 6b and 6d) which terminates just west of the three masses of supraslab seismicity and a more northeastern shallow group. Both subgroups lie away from the intense north–south band of slab seismicity (Figure 6d). The three masses of seismicity lie directly above this band (Figures 6b and 6d). Scattered seismicity with no clearly defined internal structure is largely limited to the area above and east of the three masses of seismicity and the band of intense seismicity (Figures 6c and 6d).

The lateral distance between the supraslab seismicity and the volcanic arc suggests that this seismicity is not directly related to the migration of volcanic arc fluids. Around 9% of the relocated events lie within the cluster but above the slab and outside of the other defined, spatially discrete features. These events may represent diffuse upward movement of fluids from the slab to ∼25 km depth within the overlying crust. Shallow magma chambers associated with the active arc have previously been imaged at ∼1–∼7 km directly beneath the volcanic edifice (Londoño & Kumagai, 2018) and low velocities associated with the deeper part of this system at ∼30 km depth extend no farther west than ∼75.5°W (Londoño, 2016). If this fluid represents magma feeding into the active arc, it would require near horizontal transport at mid-crustal depths across the Romeral Fault without magma escaping up this major strike-slip fault system. While possible, this seems kinematically unlikely. Instead, this seismicity may be related to the movement of non-magmatic fluids similar to those that have been previously identified >20 km trenchward of other volcanic arcs by magnetotelluric observations (e.g., Costa Rica: Worzewski et al., 2011; Chile: Cordell et al., 2019; Araya Vargas et al., 2019). Deeper investigation of these possibilities requires additional data and is beyond the scope of our study.

4.3. Temporal Patterns in Supraslab Seismicity

The earthquakes making up the three masses of seismicity ∼perpendicular to the Nazca slab discussed above occur across the full ∼decade of observations we use in our study, indicating these are persistent features of the Cauca cluster. The northern most mass of seismicity may correspond to a comparable mass of seismicity at the same depth and near the same location evident in the hypocenters obtained from teleseismic observations and plotted by Pennington (1981). If these events represent the same feature, the northern mass of seismicity has been persistent since at least the late 1960s. The duration of activity within these features is at least an order of magnitude longer than other reports of intermediate depth mantle wedge seismicity running from the top of the subducting Pacific slab to the Izu-Bonin Arc in 1985–1986 (White et al., 2019; Špičák et al., 2009) and to the Mariana Arc in 2006–2007 (White et al., 2019). The long duration of activity of the Cauca cluster suggests that these features could represent an episode or series of episodes of mainshock-aftershock sequences of seismicity on smaller-scale faults, the progressive migration of stress, or the movement of fluids through the area. To test this, we calculated new hypocenter locations for each supraslab mass covering the full 2010–2019 time period, then carried out an analysis of each mass (see Supporting Information S1 for details and Table S3 for the catalog containing the updated hypocenter locations). Initially, we attempted to plot the events' spatiotemporal distribution in each mass, but no clear trend was evident through this qualitative approach (see Figure S6; see also Figure S7 in Supporting Information S1 which shows no clear mainshock-aftershock patterns are evident at the scale of each mass in time-magnitude plots). To check for more subtle but statistically significant trends, we then attempted to track the centroid of each feature over time by sequentially binning increments of 20 time-ordered hypocenters, calculating their centroid location then advancing the increment by one hypocenter. This results in a path that moves through the core of each mass, sometime doubling back on itself as seismic activity shifts from one part of the mass to another. We then calculate 20,000 randomized re-orderings of the constituent hypocenters binned in the same way, to calculate 2σ values for the latitude, longitude, and depth of each bin's centroid. This creates a spheroidal concentration of paths that can be compared to the true, time-ordered path of each mass's centroid. We assume that statistically distinguishable from random movement of activity in each mass occurs only if the centroid spends <95% of the time steps within the calculated 2σ values in at least one dimension.

We find that statistically distinguishable from random movement of activity in at least one dimension occurs for each mass, but is most pronounced in the northern mass. The southern mass remains within the 2σ value for 99% of latitudinal and longitudinal increments and 92% of depth increments. The central mass remains within the 2σ value for ∼100% of latitudinal and depth increments, but only 89% of longitudinal increments. The northern mass remains within the 2σ value for only 91% of latitudinal increments, 83% of longitudinal increments, and 82% of depth increments. We emphasize that these measures effectively test only for the presence of coherent shifts in the distribution of seismicity within each mass on a scale of <10 km rather than random shifts. Our tests demonstrate that coherent shifts, statistically distinguishable from random shifts, are present within the cluster on the decadal scale. Presumably these shifts occur within sub-mass scale faults, however resolving progression of events along these structures is not possible with our present data set.

5. Discussion

5.1. Origin of the Cauca Cluster

Our results show that the Cauca cluster is resolvable into a set of five major features: a band of intense slab seismicity near 100 km depth within the Nazca plate's Wadati–Benioff zone, three masses of seismicity directly above this band, and a dipping plane of seismicity running from <10 km depth near the Panamá–Chocó Block suture to ∼75 km depth in the southeast part of the cluster. The key to understanding the origin of the Cauca cluster lies with the last of these features.

The spatial relationship between the Nazca plate's Wadati–Benioff zone and the shallow dipping feature could be interpreted as a double Wadati–Benioff zone, however a number of features make this untenable. Global analysis of Wadati–Benioff zone seismicity has shown the separation between the two planes of Wadati–Benioff zone seismicity increases with plate age (Brudzinski et al., 2007; Florez & Prieto, 2019). Separation between the two planes runs from 5 to 15 km for 10 Myr old plate to 15 to 25 km for 50 Myr old plate, allowing for reported uncertainties (Brudzinski et al., 2007; Florez & Prieto, 2019). Regional studies suggest that the separation between these two planes within the Nazca plate tend toward the higher side of these values. Studies of the Nazca plate at ∼18°S to ∼20°S (Comte et al., 1999; Dorbath et al., 2008; Lu et al., 2021), ∼21°S to ∼23°S (Sippl et al., 2019), and ∼30°S to ∼33°S (Marot et al., 2013) find that these segments of 35–47 Myr old plate are consistently associated with two Wadati–Benioff zone planes separated by 20–25 km. In Colombia, the age of the subducting Nazca plate is <20 Myrs, which would be expected to be associated with a separation of <10 km between the two seismic planes (Brudzinski et al., 2007; Florez & Prieto, 2019). The separation that we observe between the dipping feature and the Nazca plate's Wadati–Benioff zone is ∼25 km, well in excess of the expected separation from global observations and comparable to the separation of double planes seen in Chile in much older lithosphere. In addition, double planes of Wadati–Benioff zone seismicity consistently converge into a single feature with increasing depth, in both global studies (Brudzinski et al., 2007; Florez & Prieto, 2019) and in regional studies investigating the Nazca plate (Dorbath et al., 2008; Lu et al., 2021; Marot et al., 2013; Rietbrock & Waldhauser, 2004; Sippl et al., 2019). This contrasts with the nearly constant separation between the two features and abrupt disappearance of the upper feature in Colombia. Finally, the upper feature reaches <10 km depth within the onshore forearc while prior geophysical studies indicate the forearc's crust is >20 km (Meyer et al., 1976; Poveda et al., 2015) and the surface of the slab is at 40–50 km depth (Hayes et al., 2018; Meyer et al., 1976) at the coast, clearly indicating the upper feature lies within the overriding plate's lithosphere and is unrelated to the Nazca plate while the lower feature lies near the surface of the subducted plate.

We interpret the upper feature running from <10 km depth near the suture of the Panamá–Chocó Block to ∼75 km depth beneath the Colombian cordillera as representing the paleo-subduction interface of the block and South America. This location corresponds to the location of the paleo-triple junction where the subduction zone between the Farallon/Nazca plate and Caribbean plate intersected the Farallon/Nazca-South American subduction zone and the Caribbean-South American subduction zone around ∼40–45 Ma (Barat et al., 2014; Barbosa-Espitia et al., 2019; Buchs et al., 2019; Cardona et al., 2018; Kellogg et al., 2019; Montes et al., 2019). It is also one of the approximate points of rotation for the eastern part of the Panamá–Chocó Block during the collision and accretion of the Chocó portion of the block to South America (Barat et al., 2014). This accretion was largely completed between 17 Ma and 11 Ma (Duque-Caro, 1990; León et al., 2018; Toussaint & Restrepo, 2020).

The seismicity associated with the suture of this block shifts from a well-developed dipping feature south of a gap at 5°N to a more vertical, somewhat amorphous feature north of the gap (compare Figures 4b, 4c, 5a, and 5c). This corresponds at the surface to the shift from the southwest-northeast running Garrapatas/Istmina segment of the suture zone to the north–south running Uramita segment of the suture zone (e.g., Duque-Caro, 1990; León et al., 2018; Suárez-Rodríguez, 2007), indicating these segments have significantly different geometry at depth. Seismicity beneath the Uramita segment of the suture may be further complicated by the subduction of the Sandra Ridge and related propagation of the Caldas Tear (Martínez-Jaramillo & Prieto, 2024; Vargas & Mann, 2013) which passes beneath the suture near 5.5°N and has significant influence on both slab geometry (e.g., Sun, Bezada, et al., 2022; Wagner et al., 2017) and surface geomorphology (Pérez-Consuegra et al., 2021). The modern subducted portion of the Caribbean plate does not extend south of the Caldas Tear at depths corresponding to our observed seismicity (e.g., Kellogg et al., 2019; Sun, Bezada, et al., 2022; Syracuse et al., 2016; Vargas & Mann, 2013; Wagner et al., 2017). Therefore, we interpret the shallow, dipping plane of seismicity south of ∼5.5°N to mark a ∼180 km long subducted segment of the Panamá–Chocó Block that has been detached from the rest of the Caribbean plate following its collision with South America.

The spatial correspondence of the subducted segment of the Panamá–Chocó Block, the three masses of mantle wedge seismicity, and north–south band of intense seismicity within the Nazca slab provide a possible explanation for the unusual characteristics of Cauca cluster seismicity. The subducted segment of the block likely provides material cool enough to support brittle failure while shielding the underlying slab from the hot convecting mantle wedge, supporting greater seismicity in the Nazca slab than in the region immediately to the south. While we are aware of no other documented examples of this precise process, it may be conceptualized as analogous to what occurs at a trench-trench-trench triple junction. Thermal models of the trench-trench-trench Boso-Oki Triple Junction where the Pacific plate subducts beneath the Philippine Sea plate and the North America plate have shown that an overlying section of the Philippine Sea slab may prevent warming of the underlying Pacific slab, depressing isotherms and permitting seismicity to extend to greater depths than would be possible in the absence of the overlying slab (Ji et al., 2017). Mantle flow within the mantle wedge corner may also be significantly impacted by the presence of an overlying segment of slab (Ji et al., 2017), potentially reducing return flow within the mantle wedge corner and further cooling it (e.g., Schurr & Rietbrock, 2004). The significant complexity in shear-wave anisotropy observed beneath Cauca and adjacent regions (Idárraga-García et al., 2016; Porritt et al., 2014) reflects complex mantle flow, however any effects of the overlying Panamá–Chocó Block lithosphere cannot be clearly separated from effects attributed to the Caldas Tear (Idárraga-García, 2016; Porritt et al., 2014) or additional complexities to the south (Idárraga-García, 2016).

This interpretation suggests that the thermal structure of the region containing the Cauca cluster differs significantly from neighboring regions. Heat flow and geothermal gradient measurements for the region are very sparse (e.g., Hamza et al., 2005; Vargas et al., 2015), however the limited direct measurements in the region and estimates from Curie point depths indicate that the geothermal gradient in the intermontane basin overlying the Cauca cluster is low and comparable to the gradient of the coastal forearc basin to the southwest (Vargas et al., 2015), suggesting a relatively cold thermal structure. Indirect evidence supporting a relatively cold lithospheric structure is also provided by seismic data covering the region. An ambient noise derived S-wave tomography model for the upper to middle crust in the region (Poveda et al., 2018) shows that the mid-crust above the Cauca cluster is somewhat faster than the mid-crust of the active arc segments to the north and south. A coda attenuation tomography model to a depth of ∼100 km for the region (Vargas et al., 2019) shows that the crust and lithospheric mantle above and containing the Cauca cluster has lower seismic attenuation than neighboring regions. Both data sets are sensitive to temperature and the presence of fluid or melt, with higher S-wave velocities and lower attenuation being associated with lower temperatures and decreased amounts of fluid or melt. Taken together, these lines of evidence suggest the Cauca cluster region's lithosphere is cooler than neighboring regions.

The magmatic history of the region suggests that the Cauca region has had a cooler lithosphere little affected by arc magmatism since ∼30–40 Ma. Cretaceous to early Eocene granitoid rocks exposed within the Cordillera Central south of ∼7°N and extending into Ecuador (see compilations in Lara et al., 2018; Barbosa-Espitia et al., 2019; Leal-Mejía et al., 2019; Montes et al., 2019; George et al., 2021; Rodriguez-Corcho et al., 2022) indicate that the Colombian volcanic arc throughout our study area was continuous prior to interactions with the Panamá–Chocó Block. This contrasts with the subsequent evolution of the arc.

In the mid-to-late Eocene, the southern segment of the Colombian volcanic arc south of ∼3°N remained active while the segment to the north became inactive (Barbosa-Espitia et al., 2019; Montes et al., 2019; George et al., 2021; see also compilations in Leal-Mejía et al., 2019; Rodriguez-Corcho et al., 2022). Cessation of all arc volcanism in Colombia occurs between ∼24 and ∼40 Ma (e.g., Kellogg et al., 2019; Leal-Mejía et al., 2019; Montes et al., 2019; Rodriguez-Corcho et al., 2022), which may be due to complications from the subduction of the overthickened oceanic crust of the Caribbean plate (e.g., Bayona et al., 2012; Kellogg et al., 2019; Taboada et al., 2000) or from a switch to a transpressional regime between the Caribbean and South American plates (e.g., Bayona et al., 2012; Montes et al., 2019). We additionally note that the period between ∼28 and ∼40 Ma corresponds to a period of time of highly oblique convergence (∼45°–∼50°, assuming the ∼20° NE-SW trend of the Colombian Andes reflects the approximate orientation of the paleo trench) between the Farallon/Nazca and South American plates (Somoza & Ghidella, 2012). High convergence obliquity, especially obliquity >40°, has been suggested to significantly decrease arc volcanism (Hughes & Mahood, 2008; Rosenbaum et al., 2021; Sheldrake et al., 2020), and this may help to explain the lack of arc volcanism south of the Caribbean-Farallon/Nazca-South American triple junction.

Resumption of extensive arc volcanism to the north and south of the Colombian margin begins at ∼24 Ma (see compilations in Kellogg et al., 2019; Leal-Mejía et al., 2019; Rodriguez-Corcho et al., 2022), approximately corresponding to the breakup of the Farallon plate into the Nazca and Cocos plates (e.g., Echeverri et al., 2015; Lonsdale, 2005; Meschede & Barckhausen, 2000) and a significant decrease in subduction obliquity between the Nazca and South American plates (e.g., Echeverri et al., 2015; Somoza & Ghidella, 2012). In contrast to the continuous pre-40 Ma volcanic arc, the post-24 Ma to present volcanic arc is characterized by a lack of arc volcanism within the Cauca region (e.g., compilations in Kellogg et al., 2019; Rodriguez-Corcho et al., 2022; Wagner et al., 2017). This persistent shift in behavior following the initial interaction of the Panamá–Chocó Block with the margin suggests that the convecting mantle wedge has been displaced from the Cauca region by the subducted continuation of the block beneath the region.

Termination of subduction has previously been shown to result in fragments of down-going plates remaining attached to and laterally displaced along with unsubducted portions of plates. The best documented examples occur with fragments of the Farallon slab partially subducted beneath the North America plate in Baja California (e.g., Paulssen & de Vos, 2017; Wang et al., 2013) and central California (e.g., Dougherty et al., 2021; Jiang et al., 2018; Wang et al., 2013). In these locations, the subduction of the Pacific-Farallon spreading ridge resulted in both termination of subduction and incorporation of microplate fragments of the Farallon into the Pacific plate. In Baja California, the microplate fragment and attached small piece of subducted slab extends from the surface to between 115 and 135 km depth (Paulssen & de Vos, 2017; Wang et al., 2013). In central California, the piece of slab extends to between 150 and 200 km depth (Jiang et al., 2018; Wang et al., 2013). Both of these Farallon fragments extend to a depth comparable to the inferred end of the subducted continuation of the Panamá–Chocó Block at ∼125 km depth. Both of the Farallon fragments have also survived for a prolonged period of time in geodynamically active settings without detachment or incorporation into the convecting mantle. The microplate associated with the Baja California fragment was emplaced when subduction ceased ∼12 Ma and has since survived ∼300 km of displacement during the opening of the Gulf of California (e.g., Atwater & Stock, 1998). The microplate associated with the central California fragment was emplaced ∼18 to ∼20 Ma (Atwater & Stock, 1998; Dougherty et al., 2021; Nicholson et al., 1994; Wang et al., 2013) and the fragment itself extends eastward across the San Andreas fault (Dougherty et al., 2021; Jiang et al., 2018; Wang et al., 2013), requiring it to have survived the 820 ± 50 km of rotational and translational displacement experienced subsequently by the attached microplate (Nicholson et al., 1994). The subducted segment of the Panamá–Chocó Block has survived up to 20 Myrs longer than either of the North American examples, however numerical modeling has shown that shorter and colder slab fragments may persist for a longer time within the mantle before detachment (Burkett & Gurnis, 2013; Thielmann & Schmalhoz, 2020). Given that the base of the Panamá–Chocó Block's subducted segment is in direct contact with the subducting Nazca plate, we would expect the segment to be significantly colder than slab fragments exposed at their base to the convecting mantle. A colder temperature within the Panamá–Chocó Block's subducted segment than within the North American slab fragments may also in part explain why the block's segment is seismically active while the North American examples are aseismic. The post-accretion displacements experienced by the Panamá–Chocó Block along the Uramita and Garrapatas/Istmina Sutures are poorly constrained, however these displacements must be less than ∼500 and ∼300 km, the lengths of these sutures respectively. This displacement is comparable to or significantly less than that experienced by the North American examples.

Given the above points, we present our preferred structural interpretation for the Cauca cluster and adjacent parts of the Colombian subduction zone (Figure 7). While our interpretation is broadly similar to the structures proposed by Taboada et al. (2000) and Bayona et al. (2012) north of our study area beyond the Caldas Tear, we emphasize that the patterns of seismicity in the Cauca region differ greatly from the largely aseismic slab or slabs present to the north and that our interpretation does not necessarily imply continuity between the subducted part of the Panamá–Chocó Block and other Caribbean plate material. South of the cluster (Figure 7a), no significant part of the Panamá–Chocó Block extends into the mantle and the convecting mantle wedge is unobstructed, allowing arc volcanism and a normal forearc thermal structure. Within the cluster (Figure 7b), the extension of the Panamá–Chocó Block lies directly above the subducting Nazca plate. This displaces the convecting mantle wedge, disrupting mantle wedge corner flow which may already be reduced in this location due to high convergence

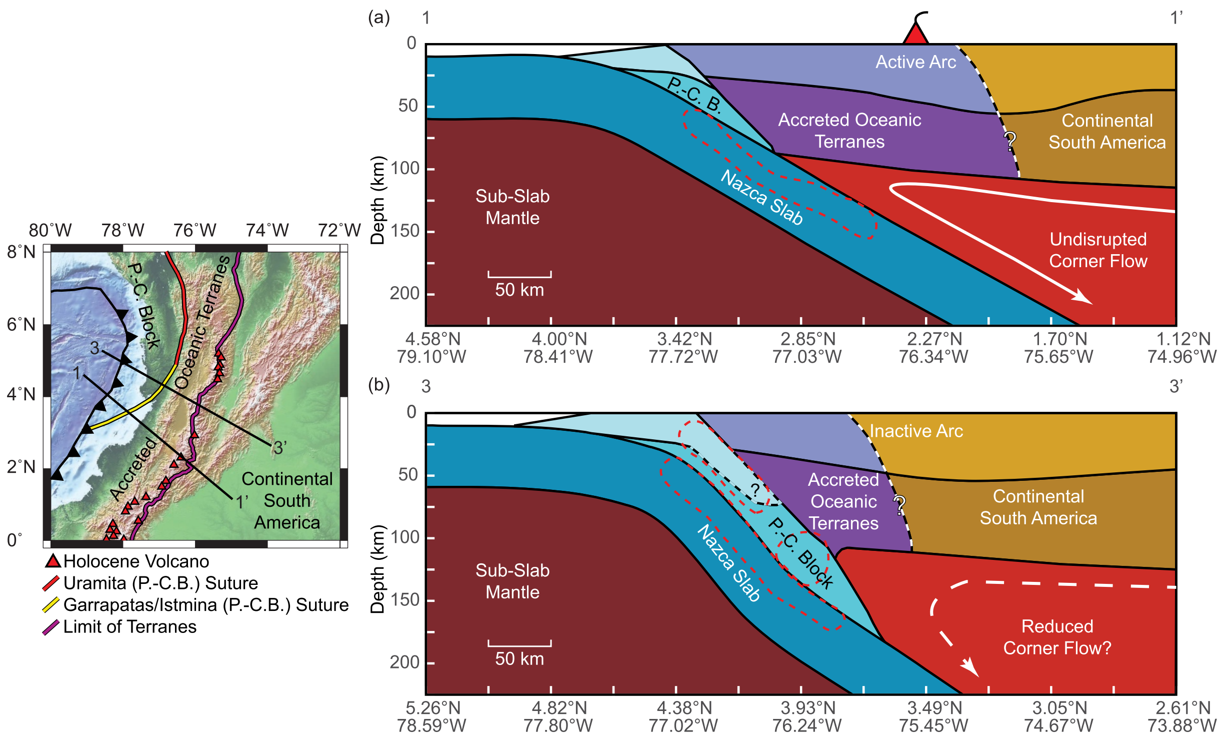

Figure 7. Block model interpretation of the region south of the Cauca cluster corresponding to cross-section line 1-1' (Figures 2a and 4a), and the southern portion of the Cauca cluster corresponding to cross-section line 3-3' (Figures 2c and 4c). Red dashed lines mark locations of areas of slab and key supraslab seismicity from Figures 4a and 4c. Blocks represent lithosphere-scale units of overriding plate and the slab. We assign a westward vergence to the Panamá–Chocó suture based on the observed dipping plane of seismicity in our results (consistent with Colmenares et al., 2019's much shallower structures along this suture). We follow Cediel et al. (2003) and Colmenares et al. (2019) in assigning a westward vergence to the suture between the accreted oceanic terranes and continental South America, however this geometry is uncertain and an eastward verging suture is possible (e.g., Bourgois et al., 1982; Kellogg & Vega, 1995). Approximate Mohorovičić discontinuity depths (black line separating lighter crust and darker lithospheric mantle in cross-sections) are after Poveda et al. (2015) and South American lithosphere-asthenosphere boundary is after Blanco et al. (2017). See text for discussion.

obliquity (Rosenbaum et al., 2021) and producing a gap in the Colombian volcanic arc. The presence of the block thus significantly disrupts the forearc thermal structure, keeping the slab cooler to a greater depth than in the south and providing cold material for seismicity to occur within and above the slab. Near the downdip edge of the block temperatures are likely to rapidly increase, possibly promoting dehydration of the slab and the release of slab fluids in the north–south trending band of intense seismicity within the slab (Figure 6d). These fluids would then rise into the overlying block. Near the warmer downdip edge of the block, the fluids would encounter lithosphere too hot to stabilize antigorite (>∼600°C–650°C at the depths of interest (Hacker, Abers, & Peacock, 2003; Reynard, 2013)), permitting the fluids to persist as a free phase and drive or enhance seismicity as discussed in the next section. Fluids released from the slab closer to the trench or continuing to rise above the masses of seismicity within the Cauca cluster would encounter lithosphere sufficiently cool to stabilize antigorite and some fraction of the fluids could be consumed to form this mineral. Any deformation within the region with stable antigorite would likely occur through an aseismic or slow-slip mechanism (e.g., Burdette & Hirth, 2022; Ferrand et al., 2017; French et al., 2019; Gasc et al., 2017; Goswami & Barbot, 2018; Okazaki & Katayama, 2015) which would be undetectable with our data set.

5.2. Implications for Causes of Intermediate Depth Seismicity

The occurrence of Cauca cluster seismicity within the cold lithosphere of the subducted continuation of the Panamá–Chocó Block at intermediate (>70 km) depth provides unique constraints on viable mechanisms of intermediate depth seismicity. As the continuation of the block has been largely stationary for at least the last ∼12 million years and potentially the last ∼40 million years (see above discussion), neither dehydration embrittlement (e.g., Hacker, Peacock, et al., 2003; Jung & Green, 2004; Peacock, 2001) nor dehydration-driven stress transfer (e.g., Ferrand et al., 2017; Kita & Ferrand, 2018) can be invoked as likely causes for seismicity. Both of these

10.1029/2024JB030067

mechanisms require the breakdown of hydrous mineral phases in the source region of intermediate depth earthquakes and cannot recur along the same fault segment repeatedly. Examination of slab seismicity within the Cauca cluster allows us to estimate the approximate time any hydrated material within the subducted continuation of the Panamá–Chocó Block should have taken to fully dehydrate. Dehydration reactions relevant for a subducted oceanic plate are largely insensitive to pressure (Hacker, Abers, & Peacock, 2003), and for a given depth in the Cauca cluster, the slab will be colder than the subducted segment of the block. This means that if dehydration is assumed to be responsible for the observed seismicity in the Cauca cluster, any depth at which the slab is seismically active exists under pressure-temperature conditions in which hydrous minerals are unstable and that the Panamá–Chocó Block at the same depth will also exist under unstable conditions. The time taken by a segment of the slab to move from the depth at which slab seismicity begins (∼50 km) to the depth at which slab seismicity ends (∼150 km) thus provides an approximate estimate of how much time the block would require to dehydrate. Given an observed slab dip between ∼35° and ∼40° and a convergence rate of 6.0 cm/yr, dehydration within the slab takes between 2.6 and 2.9 Myrs. If dehydration reactions were directly responsible for Cauca cluster seismicity, dehydration would have run to completion long before the present.

Three alternate possibilities for the causes of Cauca cluster supraslab seismicity are viable given the configuration of the slab and overlying Panamá–Chocó Block. (a) Supraslab seismicity may be driven by fluids rising from the slab into a part of the overlying block, encouraging hydrofracture within partially serpentinized mantle at a temperature near the stability limit of antigorite or within likely metasomatized mantle at a temperature beyond the stability limit of antigorite but below temperatures at which basaltic melt can be generated by the interaction of slab fluids and mantle material. (b) Supraslab seismicity occurs within the unusually cold cores of incipient subducted sediment diapirs detaching from the subduction channel as it moves out from beneath the cold and therefore highly viscous lithosphere of the subducted Panamá–Chocó Block into the less viscous convecting mantle wedge. (c) Supraslab seismicity may be driven by focusing of deformation within a relatively restricted area at the downdip edge of the block driven by coupling with the convecting mantle wedge, analogous to slab necking. This localization of deformation may encourage thermal shear instability.

5.2.1. Seismicity Driven by Hydrofracture?

Hydrofracture has previously been proposed both as a possible means of fluid movement within the mantle (e.g., Nicolas, 1986; Dahm, 2000; and see review by Kohlstedt & Holtzman, 2009) and as a possible explanation for at least some intermediate depth seismicity (e.g., Davies, 1999; White et al., 2019), however both the general lack of reported seismicity within mantle wedges at intermediate depth and theoretical considerations (e.g., Kelemen et al., 1997; and review by Kohlstedt & Holtzman, 2009) make explanations relying on this mechanism problematic. The unique and extensive presence of supraslab, mantle wedge seismicity in the Cauca cluster has previously been suggested to be driven by hydrofracture (Chang et al., 2017; Chang et al., 2019) and here we provide a more developed explanation of why this mechanism is viable for the cluster in contrast to other mantle wedge settings.

We begin by examining the equation describing hydrofracture (following Daines & Pec, 2015):

$$T_s \leq (\rho_s - \rho_f)\, g \delta_c \tag{1}$$

here T_s is the tensile strength of the mantle rock hosting the fluid, ρ_s is the density of this mantle rock, ρ_f is the density of the fluid, g acceleration due to gravity, and δ_c is the compaction length. For hydrofracture to occur, T_s must be less than or equal to the combined effects of a fluid's buoyancy relative to the mantle and compaction length, a parameter reflecting the combined material properties of the fluid and its matrix which represents the characteristic length over which compaction rate decreases an arbitrary amount (McKenzie, 1984). For a mantle rock, T_s is on the order of ≥50 MPa (Kelemen et al., 1997).

Examining buoyancy first, we assume that mantle rock has a density of 3,300 kg/m^3. Between 2 and 3 GPa (equivalent to ∼70 and ∼105 km depth), hydrous basaltic and andesitic melts range in density from ∼2,500 to ∼2,800 kg/m^3, anhydrous basaltic and andesitic melts range from ∼2,700 to 3,000 kg/m^3 (Ueki & Iwamori, 2016), and slab derived aqueous fluids range from ∼1,200 to 1,300 kg/m^3 (Hack & Thompson, 2011; Manning, 2004; Manning & Frezzotti, 2020). This yields a density contrast of 300 to 1,000 kg/m^3 for silicic melts relative to the mantle and 2,000 to 2,100 kg/m^3 for aqueous fluids relative to the mantle. These values require that the compaction length be at least between 2.4 and 2.5 km for aqueous fluids, between 6.4 and 10 km for hydrous silicic melts, and between 8.5 and 17 km for anhydrous melts in order to induce hydrofracture. The generally much lower values of compaction length here compared to the value of 10 km calculated by Kelemen et al. (1997) for a spreading ridge or hot spot setting highlight the critical role that water plays in a subduction setting in rendering hydrofracture a viable cause of mantle wedge seismicity.

The importance of water is further highlighted when compaction length itself is examined. Compaction length, δ_c, is described in terms of the effective bulk viscosity ζ, effective shear viscosity η, the viscosity of the fluid μ, and permeability K by the following equation (Daines & Pec, 2015):

$$\delta_c = [((\zeta + (4/3)\eta)/\mu)K]^{1/2} \tag{2}$$

Empirical measurement and numerical modeling (see compilation in Hack & Thompson, 2011 and references therein) have constrained the viscosity of aqueous slab fluids to be $\sim 10^{-4}$ Pa s (Hack & Thompson, 2011; Manning & Frezzotti, 2020) and the viscosity of hydrous melts to be between $\sim 10^1$ and $\sim 10^2$ Pa s (Hack & Thompson, 2011) for the relevant range of pressures. Other parameters determining compaction length are less constrained and require additional assumptions.

Effective bulk and shear viscosities of a melt-bearing material are dependent on the composition of the material, grain size of the material, its temperature, and the amount of melt present (e.g., Kelemen et al., 1997; Schmeling et al., 2012; Takei & Holtzman, 2009). We simplify this by assuming the composition, grain size, and temperature of the material an aqueous fluid and hydrous melt move through are identical. As the process of hydrofracture will occur where fluid fractions are around a few (<10) precent and permit the escape of excess fluid (Reynard et al., 2011; Richard et al., 2007), we may further assume that the effective viscosities and permeability of the material are a function of the dihedral angle of the fluid and any mineral phases present (on dihedral angle and effective viscosities see Takei (1998), Schmeling et al. (2012); on dihedral angle and permeability see von Bargen and Waff (1986), Wark et al. (2003)). A maximum dihedral angle of <60° is necessary to form an interconnected network of fluid within a matrix of mineral grains (e.g., Daines & Pec, 2015; Holness, 1997) and smaller dihedral angles result in both lower effective bulk and lower effective shear viscosities (Schmeling et al., 2012; Takei, 1998). Dihedral angles for the olivine-orthopyroxene-melt system at 1.5–2.5 GPa average between ∼20° and ∼40° (Fujii et al., 1986; von Bargen & Waff, 1988). Dihedral angles for the comparable olivine-orthopyroxene-CO_2 and NaCl bearing H_2O system (a fluid composition similar to that of slab derived fluids, see Manning, 2004) at similar pressures range from ∼40° to ∼55° (Huang et al., 2020).

These dihedral angle values may be used to determine the approximate, relative effective viscosities and permeability of the two fluid bearing systems. For 3%–5% fluid fraction, the relative effective bulk viscosity differs by at most 10^1 while the relative effective shear viscosity differs by around 10^0 (Schmeling et al., 2012). For the same range of fluid fraction, permeabilities for the two ranges of dihedral angle are nearly identical (Wark et al., 2003).

We exploit these relative effective viscosities and the permeability to define a ratio for the compaction length of the two fluids:

$$\delta_{ca}/\delta_{cm} = \left[(34/3)/\mu_a\right]^{1/2} / \left[(7/3)/\mu_m\right]^{1/2} \tag{3}$$

where δ_{ca} and μ_a are the compaction length and fluid viscosity for the aqueous fluid case, respectively, and δ_{cm} and μ_m are the equivalent for the melt case. Substituting the fluid viscosities mentioned above for the two cases yields an aqueous fluid compaction length equivalent to between ∼700 and ∼2,200 times the compaction length of the hydrous melt.

The 10^2 to 10^3 times greater compaction length for aqueous slab fluids than for hydrous silicic melt make hydrofracture much more likely for any composition or temperature of the surrounding rock, so long as the temperature is below the rock's wet solidus. As lower temperatures increase the effective viscosity and compaction length of a material (Kelemen et al., 1997), rock in which slab fluids are stable would tend to further promote hydrofracture relative to rock in which melts are stable. We note here that the reported dihedral angles for antigorite and aqueous fluid are ∼52° (Wang et al., 2017) and that its viscosity is $\sim 4 \times 10^{19}$ Pa s (Hilairet

Table 1
Isotropic Seismic Properties of Materials Potentially Hosting Cauca Supraslab Seismicity at 3 GPa

Material	P-wave velocity (km/s)	S-wave velocity (km/s)	Vp/Vs ratio	Reference
Olivine-Rich Peridotite	~7.65–8.2	~4.3–4.65	~1.76–1.78	Hacker and Abers (2012)
Antigorite	~6.26–6.5	~3.3	~1.9	Wang et al. (2019)
Orthopyroxene	~7.3–8.0	~4.3–4.7	~1.70–1.72	Hacker and Abers (2012)
Coesite	~8.0	~4.6	~1.75	Abers and Hacker (2016)
α-Quartz	~5.3–6.2	~3.7–4.0	~1.43–1.55	Abers and Hacker (2016)
β-Quartz	~6.4–7.3	~4.0–4.2	~1.59–1.76	Abers and Hacker (2016)
Talc	~6.95	~4.0	~1.74	Peng et al. (2022)
Chlorite	~5.0–6.0	~2.4–2.6	~2.15–2.37	Manthilake et al. (2021)
Serpentine-Dominated Mélange	~6.2–7.1	~3.5–4.0	~1.78–1.80	Codillo et al. (2018) [a]; Abers and Hacker (2016)
Sediment-Dominated Mélange	~7.6–7.9	~4.2–4.5	~1.76–1.79	Codillo et al. (2018) [a]; Abers and Hacker (2016)
Limestone (Aragonite)	~6.7	~3.5	~1.9	Sun, Li, et al. (2022)
Jadeite	~8.86	~5.12	~1.73	Hao et al. (2020)

[a]Modal mineralogy wt. % for serpentine- and sediment-dominated mélange from Codillo et al. (2018) were approximated to the closest equivalents available in Abers and Hacker (2016) model, reported values represent high and low extremes obtained using 500°C–1100°C temperature range and endmembers for minerals with solid-solution series.

et al., 2007) which is comparable to the viscosity of a water-saturated, unserpentinized olivine (Dixon et al., 2004). Comparative study of harzburgite and dunite compositions deformed under the same geologic conditions has further shown that increasing the amount of orthopyroxene in a peridotite causes a less than 10^1 increase in the viscosity of the peridotite (Hansen & Warren, 2015). These characteristics indicate hydrofracture due to aqueous fluids within cool material like that of the subducted Panamá–Chocó Block is much more likely than hydrofracture due to melt within a typical mantle wedge setting, regardless of the block's degree of serpentinization or metasomatism.

If hydrofracture is the cause of supraslab seismicity within the Cauca cluster, the long-term flux of fluid through the material overlying the slab may lead to compositional changes within the material hosting the cluster. Assuming the majority of this material was originally a peridotite, prolonged interaction with fluids would result in compositions ranging from those dominated by antigorite if the fluid is silica-free and the temperature is below <650°C to those dominated by a combination of enstatite, quartz, and possibly a significant amount of talc if the fluid is silica-bearing and temperatures >650°C (Peacock & Wang, 2021). While serpentine minerals like antigorite have generally been shown to deform aseismically (e.g., Chernak & Hirth, 2010; Hilairet et al., 2007), recent experimental observations have shown that localized, semi-brittle deformation and related breakdown is possible in antigorite even under pressures and temperatures where the mineral is nominally stable near its high temperature stability limit (~500°C–650°C, see e.g., Gasc et al., 2017; French et al., 2019; though strain rate may also be important, see Burdette and Hirth (2022)). Continued fluid flux through the material could then re-serpentinize this material, in contrast to the dehydration conditions described above in Section 5.2. This suggests that we cannot exclude the antigorite endmember from acting as a possible host for Cauca cluster seismicity.

Future observations of the earthquake source characteristics and the material properties of the source region are necessary to test for hydrofracture. While prior work (e.g., Chang et al., 2019) has examined focal mechanisms in the cluster, no effort was made to constrain the degree of volumetric change associated with these events. Observation of volumetric change would be strong support for the hydrofracture explanations. Less direct evidence could also be obtained by calculating the P-wave velocities, the S-wave velocities, and the Vp/Vs ratio for the material encompassing the supraslab earthquakes (see Table 1). While anisotropy may complicate these values (e.g., Hacker & Abers, 2012; Peng et al., 2022), Table 1 illustrates how both a hydrous antigorite endmember and silica-enriched endmember may be clearly distinguished with these three parameters. Existing receiver function results for the Cauca region are too coarse to image features on the scale of the supraslab masses of seismicity we observe, however the weak velocity contrast across the continental Mohorovičić discontinuity overlying the region (Mojica Boada et al., 2022) is potentially consistent with the low S-wave velocities associated with antigorite, α-quartz or talc. Hydrofracture in a variety of other settings has been associated with unusually low Vp/Vs ratio values that cannot be easily explained by rock composition alone (e.g., Chatterjee et al., 1985; Huesca-Pérez et al., 2021; Lin & Shearer, 2009; Tan et al., 2020), which may relate to the presence of water-filled cracks with large aspect ratios in hydrofracture settings (see discussion in Shearer, 1988; Lin & Shearer, 2009 as well as Takei, 2002), and as such extremely low Vp/Vs ratio values may not rule out a hydrofracture explanation.

5.2.2. Seismicity Driven by Deformation at the Core of Sediment Diapirs?

Subduction mélange, a mix of subducted sediments, fragments of slab oceanic crust, and hydrated mantle material, play an important role in subduction zone processes (e.g., Behr & Bürgmann, 2021). At > ∼ 50 km depth mélange represents a cold, buoyant material with respect to the overlying mantle which may be capable of forming cold diapirs that rise from the subducting slab and ultimately feed arc volcanism (e.g., Cruz-Uribe et al., 2018; Klein & Behn, 2021; Marschall & Schumacher, 2012). Recent petrologic studies of the northern segment of the Colombian volcanic arc, immediately convergence-ward of the Cauca cluster, have suggested that mélange diapirs may be present in the region at ∼80–120 km depth (Errázuriz-Henao et al., 2019; Errázuriz-Henao et al., 2021). The correspondence in depth between these proposed mélange diapirs and the masses of seismicity we observe extending from the slab, as well as similarities in the geometry of this seismicity and the geometry of numerically modeled cold diapirs (e.g., Ghosh et al., 2020; Zhu et al., 2009) suggests that these masses of seismicity could occur within cold diapirs.

Mélange diapirs have been suggested to be a process operating at many subduction zones (e.g., Codillo et al., 2018; Cruz-Uribe et al., 2018; Marschall & Schumacher, 2012; Nielsen & Marschall, 2017), and the lack of supraslab seismicity comparable to that observed in Colombia at other locations suggests that an unusual process is operating in the Cauca region. Numerical modeling has indicated that both the temperature of the mélange and the ratio of the viscosities of the mélange and the overlying mantle are important factors in diapir formation (Klein & Behn, 2021; Miller & Behn, 2012). Material within the subduction channel which passes beyond the downdip edge of the subducted portion of the Panamá–Chocó Block would be exposed to a rapid increase in temperature and a rapid decrease in the viscosity of the overlying mantle wedge. Both changes are associated with diapir formation (Miller & Behn, 2012), and these sudden shifts near the end of the block may act to focus diapir formation in this location. Seismicity associated with a mélange diapir is likely to be greatest during its formation rather than after it has detached from the slab as this will be when its core is both at its coldest (as low as 500–700°C; Miller & Behn, 2012 and see temperature evolution in Zhang et al., 2020) and experiencing a high strain rate. This temperature range corresponds to the 500–700°C window for jadeitite formation and associated hydrofracture proposed by Angiboust et al. (2021) to explain instances of supraslab mantle wedge seismicity observed at up to ∼50 km depth (e.g., Davey & Ristau, 2011; Halpaap et al., 2019; Laigle et al., 2013; Nakajima & Uchida, 2018). We note here that experimental measurement of clinopyroxene(jadeite)-clinopyroxene(jadeite)-aqueous fluid dihedral angles for the relevant range of temperatures and pressures is well above the 60° cutoff for the formation of an interconnected fluid network (Mibe et al., 2003) that allows hydrofracture (see Section 5.2.1), which argues against the viability of this mechanism without significant decreases in dihedral angle like those observed for other minerals with multicomponent fluids (e.g., H_2O-CO_2 or H_2O-CO_2-NaCl fluids for olivine/orthopyroxene in Huang et al., 2020). Assuming this objection can be overcome, jadeitite formation would be a good candidate for hydrofracture within a diapir. Jadeitite makes up a significant portion of exhumed subduction zone mélange material (e.g., Harlow et al., 2015; Marschall & Schumacher, 2012) and its mechanism of formation is tied to processes within mélange material or to ultramafic material adjacent to mélange material (see Angiboust et al., 2021 and reviews by Harlow et al., 2015; Harlow & Sorensen, 2005). Jadeitite incorporated into or formed within unusually cold cores of mélange diapirs may explain supraslab seismicity in the Cauca cluster, making this seismicity directly analogous to the shallower mantle wedge seismicity in Angiboust et al.'s (2021) model.

The composition of a subduction zone mélange diapir at ∼100 km depth is likely to be complicated. The presence of seismicity would suggest a significant jadeitite component is present, and buoyancy considerations suggest that little to no high-density slab derived basalt (eclogite) would be present. Identifiable rock bodies in mélange exposed at the surface often include a significant amount of near monomineralic chlorite schist (Marschall & Schumacher, 2012), and petrologic high pressure experiments have demonstrated that chlorite in mélange can be stable up to 650–850°C at 2–3 GPa (Lakey & Hermann, 2022) depending on the amount of magnesium incorporated, indicating it may also form a significant component of mélange diapir cores prior to their dehydration. In

Colombia, evidence for significant carbonate sediment subduction has been detected in volcanic material hypothesized to derive from mélange material (Errázuriz-Henao et al., 2019), which at our depth of interest would be represented by aragonite (Zhao et al., 2019). We assume that the non-carbonate component of the subducted sediment in Colombia is broadly comparable to the sediment-dominated or serpentinite-dominated mélange analyzed by Codillo et al. (2018).

As this explanation can be considered a mechanically identical but geologically distinct variation of the mechanism outlined in Section 5.2.1, we focus here on observations that would distinguish hydrofracture within subduction mélange diapirs from hydrofracture within the altered forearc mantle materials discussed above. P-wave, S-wave, and Vp/Vs ratio (Table 1) values for serpentine, aragonite, or chlorite dominated mélange compositions may be largely indistinguishable from a partially serpentinized mantle wedge, though a composition extremely rich in chlorite would be distinct. If the intense seismicity observed in the Cauca cluster is associated with the formation of jadeitite, distinctively high values of P-wave and S-wave velocities with moderate Vp/Vs ratio values should be observed. Extensive deformation should occur during formation of a diapir, and given the high degree of seismic anisotropy possible in chlorite (Manthilake et al., 2021), antigorite (e.g., Hacker & Abers, 2012; Wang et al., 2019), and jadeite (Hao et al., 2020) this deformation should result in extreme anisotropy along seismic ray paths passing through the supraslab clusters of seismicity relative to adjacent regions. This is likely to contrast with the hydrofracture mechanism outlined in 5.2.1 where little to no significant movement of rock material is required. While more observations are needed, the two stations in the SGC array that sit nearly on top of the northern and southern supraslab clusters of seismicity show evidence of less supraslab anisotropy than stations located well south of the Cauca cluster (Idárraga-García et al., 2016), inconsistent with mélange diapir model's predictions.

5.2.3. Seismicity Driven by Strain Localization and Thermal Shear Instability?

Downdip of the megathrust and updip of the convecting mantle wedge, the interface between subducting slab and overriding forearc is believed to be decoupled due to changes in the relative strength of minerals in the subduction channel and overlying mantle controlled at least in part by temperature (e.g., Wada et al., 2008; Wada & Wang, 2009; Syracuse et al., 2010; Tan, 2017; Arcay, 2017; Agard et al., 2020; though see review by Abers et al., 2020 for a contrasting view). Increase in temperature as the slab approaches the convecting mantle wedge would both weaken the overlying mantle material (e.g., Wada & Wang, 2009; Wada et al., 2008) and trigger changes in the mineral phases that decouple the slab from overlying material (e.g., Agard et al., 2020; Arcay, 2017). This would allow the slab and overlying material to couple, driving corner flow and entraining mantle material with the downgoing slab (e.g., Agard et al., 2020; Wada et al., 2008). In most mature subduction zones, the point of coupling stabilizes at ~80–100 km depth, however in the Cauca region the presence of the subducted portion of the Panamá–Chocó Block may have cooled the subduction zone enough to push this point deeper. Gradual heating at the block's downdip edge may allow this point to migrate trenchward over time, allowing coupling between the downdip edge and the underlying slab. If so, a rapid increase in stress along the block's base would occur at this coupling point, promoting strain within both the overlying block and underlying slab. This may lead to progressive necking, detachment, and entrainment of the block's downdip edge, the first phase of which may be partially expressed in our observed supraslab seismicity.

Necking of material is a fundamentally ductile process, however ductile deformation within rock at ultra-high pressure conditions is capable of being localized by thermal shear runaway into very narrow shear zones. This has been identified as a potential cause of seismicity in petrophysical modeling (Hobbs & Ord, 1988; John et al., 2009; Kelemen & Hirth, 2007; Ogawa, 1987; Thielmann et al., 2015), high pressure laboratory studies (e.g., Ohuchi et al., 2017), and studies of pseudotachylyte in exhumed material (e.g., Andersen et al., 2008; Deseta et al., 2014; John et al., 2009). Areas of intense, intermediate depth seismicity geologically and geodynamically associated with the termination of subduction and slab detachment are frequently linked to thermal shear runaway during slab necking and detachment (see examples from the Hindu Kush: Lister et al., 2008; Poli, Prieto, Rivera, & Ruiz, 2016; Zhan & Kanamori, 2016; Kufner et al., 2021; Vrancea/Carpathians: Ismail-Zadeh et al., 2012; and Gibraltar Strait: Sun & Bezada, 2019).

If thermal shear runaway is responsible for the Cauca cluster's supraslab seismicity, it should be readily distinguishable from hydrofacture within metasomatized mantle material or subduction mélange diapirs discussed in Sections 5.2.1 and 5.2.2. No significant volumetric change should be observable in focal mechanisms calculated for the events, and they would likely occur within typical mantle peridotite rather than within material with unusual seismic velocity characteristics (compare values for olivine-rich peridotite with other entries in Table 1). High stress drop or significant changes in dynamic stress, low radiation efficiency, and slow rupture velocities, would also be expected for earthquakes generated by thermal shear runaway, as has been reported in other settings where the mechanism is believed to operate (e.g., Prieto et al., 2013; Poli, Prieto, Rivera, & Ruiz, 2016; Poli, Prieto, Yu, et al., 2016; Prieto et al., 2017; Mirwald et al., 2019)—which would not be expected for other mechanisms.

6. Conclusions

The relocation of 6,722 earthquakes within Colombia's Cauca cluster and adjacent regions exhibits 10 km-scale structures within the mantle wedge above a band of intense, depth transgressive seismicity within the subducted Nazca plate from ∼80 to 150 km depth. Major supraslab structures are a second planar, southeastward dipping feature running from ∼10 to ∼80 km depth and three, ∼20–30 km diameter masses of seismicity directly above and perpendicular to the band of seismicity in the Nazca plate. The southeast dipping feature runs from beneath the suture between South America and the Panamá–Chocó Block to the approximate center of a gap in the active volcanic arc. The three masses of seismicity lie downdip of the southward dipping feature. These features appear to respectively mark the top and downdip edge of a subducted continuation of the lithosphere of the Panamá–Chocó Block. This lithosphere has prevented contact between the hot asthenosphere of the mantle wedge and the subducting slab to >125 km depth and provided a relatively cold location for supraslab seismicity to occur within.

This configuration can be inferred to have persisted since at least 12 Ma when the block was sutured to South America. This means that the block should be at or near thermal steady state and experience no change in pressure, greatly limiting the possible mechanisms for intermediate depth seismicity compared to a subducting slab. Only three proposed mechanisms for intermediate seismicity can be viable under these conditions: hydrofracture from escaping slab-derived fluids, brittle fracture at the cores of diapirs of buoyant subduction mélange, or shear-induced thermal runway during necking of the deepest segment of the block due to coupling of the block with the slab or convecting mantle wedge. Hydrofracture would represent the least destructive of the three mechanisms to the long-term structural stability of the block, and we favor this explanation given the block's longevity.

The Cauca cluster's seismicity, the >10 million year disruption of the mantle wedge thermal structure it requires, and the localized hydration of the overlying plate it implies, reveals the degree to which terrane accretion may have a profound effect on a subduction system greatly post-dating suturing and the general resumption of normal subduction along a convergent margin.

Data Availability Statement

HypoDD (Waldhauser & Ellsworth, 2000) version 1.3 was used to calculate the earthquake relocations presented in this study. This version was obtained from and is freely available from Waldhauser and Ellsworth (2010). Questions regarding this software can be addressed to Felix Waldhauser (Columbia University). *P*-wave and *S*-wave arrival time picks for earthquakes analyzed in this study are freely available from the SGC's seismic catalog (Servicio Geológico Colombiano, 1993a), note that events prior to March 2018 are available only as SEISAN S-files and events after March 2018 are available only as QuakeML files. Relocated hypocenter locations calculated for this study are available as a catalog in Tables S2 and S3.

Acknowledgments

This work was supported by National Science Foundation Grant EAR-1760802. We also thank the staff of the SGC for assistance in accessing the SGC earthquake catalog. We thank Rachel Abercrombie, James Kellogg, Doriane Drolet, and two anonymous reviewers for providing comments that greatly strengthened this paper.

References

Abers, G. A., & Hacker, B. R. (2016). A MATLAB toolbox and excel workbook for calculating the densities, seismic wave speeds, and major element composition of minerals and rocks at pressure and temperature. *Geochemistry, Geophysics, Geosystems*, *17*(2), 616–624. https://doi.org/10.1002/2015GC006171

Abers, G. A., van Keken, P. E., & Wilson, C. R. (2020). Deep decoupling in subduction zones: Observations and temperature limits. *Geosphere*, *16*(6), 1408–1424. https://doi.org/10.1130/GES02278.1

Agard, P. (2021). Subduction of oceanic lithosphere in the Alps: Selective and archetypal from (slow-spreading) oceans. *Earth-Science Reviews*, *214*, 103517. https://doi.org/10.1016/j.earscirev.2021.103517

Agard, P., Prigent, C., Soret, M., Dubacq, B., Guillot, S., & Deldicque, D. (2020). Slabitization: Mechanisms controlling subduction development and viscous coupling. *Earth-Science Reviews*, *208*, 103259. https://doi.org/10.1016/j.earscirev.2020.103259

Andersen, T. B., Mair, K., Austrheim, H., Podladchikov, Y. Y., & Vrijmoed, J. C. (2008). Stress release in exhumed intermediate and deep earthquakes determined from ultramafic pseudotachylyte. *Geology*, *36*(12), 995–998. https://doi.org/10.1130/G25230A.1

Angiboust, S., Muñoz-Montecinos, J., Cambeses, A., Raimondo, T., Deldicque, D., & Garcia-Casco, A. (2021). Jolts in the jade factory: A route for subduction fluids and their implications for mantle wedge seismicity. *Earth-Science Reviews*, *220*, 103720. https://doi.org/10.1016/j.earscirev.2021.103720

Angiboust, S., & Raimondo, T. (2022). Permeability of subducted oceanic crust revealed by eclogite-facies vugs. *Geology*, *50*(8), 964–968. https://doi.org/10.1130/G50066.1

Araya Vargas, J., Meqbel, N. M., Ritter, O., Brasse, H., Weckmann, U., Yáñez, G., & Godoy, B. (2019). Fluid distribution in the Central Andes subduction zone imaged with magnetotellurics. *Journal of Geophysical Research: Solid Earth*, *124*(4), 4017–4034. https://doi.org/10.1029/2018JB016933

Arcay, D. (2017). Modelling the interplate domain in thermo-mechanical simulations of subduction: Critical effects of resolution and rheology, and consequences on wet mantle melting. *Physics of the Earth and Planetary Interiors*, *269*, 112–132. https://doi.org/10.1016/j.pepi.2017.05.008

Arcila, M., & Muñoz-Martín, A. (2020). Integrated perspective of the present-day stress and strain regime in Colombia from analysis of earthquake focal mechanisms and geodetic data. In J. Gómez & A. O. Pinilla-Pachon (Eds.), *The geology of Colombia, volume 4 Quaternary, Publicaciones Geológicas Especiales* (Vol. 38, pp. 549–569). Servicio Geológico Colombiano. https://doi.org/10.32685/pub.esp.38.2019.17

Ariza-Acero, M. M., Spikings, R., Beltrán-Triviño, A., Ulianov, A., & von Quadt, A. (2022). Geochronological, geochemical and isotopic characterisation of the basement of the Chocó-Panamá Block in Colombia. *Lithos*, *412–413*, 106598. https://doi.org/10.1016/j.lithos.2022.106598

Atwater, T., & Stock, J. (1998). Pacific-North America plate tectonics of the Neogene Southwestern United States: An update. *International Geology Review*, *40*(5), 375–402. https://doi.org/10.1080/00206819809465216

Barat, F., de Lépinay, B. M., Sosson, M., Müller, C., Baumgartner, P. O., & Baumgartner-Mora, C. (2014). Transition from the Farallon plate subduction to the collision between South and Central America: Geological evolution of the Panama Isthmus. *Tectonophysics*, *622*, 145–167. https://doi.org/10.1016/j.tecto.2014.03.008

Barbosa-Espitia, Á. A., Kamenov, G. D., Foster, D. A., Restrepo-Moreno, S. A., & Pardo-Trujillo, A. (2019). Contemporaneous Paleogene arc-magmatism within continental and accreted oceanic arc complexes in the northwestern Andes and Panama. *Lithos*, *384–349*, 105185. https://doi.org/10.1016/j.lithos.2019.105185

Bayona, G., Cardona, A., Jaramillo, C., Mora, A., Montes, C., Valencia, V., et al. (2012). Early Paleogene magmatism in the northern Andes: Insights on the effects of oceanic plateau–continent convergence. *Earth and Planetary Science Letters*, *331–332*, 97–111. https://doi.org/10.1016/j.epsl.2012.03.015

Behr, W. M., & Bürgmann, R. (2021). What's down there? The structures, materials and environment of deep-seated slow slip and tremor. *Philosophical Transactions of the Royal Society A Mathematical, Physical and Engineering Sciences*, *379*(2193), 20200218. https://doi.org/10.1098/rsta.2020.0218

Bie, L., Rietbrock, A., Hicks, S., Allen, R., Blundy, J., Clouard, V., et al. (2020). Along-arc heterogeneity in local seismicity across the Lesser Antilles subduction zone from a dense ocean-bottom seismometer network. *Seismological Research Letters*, *91*(1), 237–247. https://doi.org/10.1785/0220190147

Bilek, S. L., & Lay, T. (2018). Subduction zone megathrust earthquakes. *Geosphere*, *14*(4), 1468–1500. https://doi.org/10.1130/GES01608.1

Bishop, B. T., Cho, S., Warren, L., Soto-Cordero, L., Pedraza, P., Prieto, G. A., & Dionicio, V. (2023). Oceanic intraplate faulting as a pathway for deep hydration of the lithosphere: Perspectives from the Caribbean. *Geosphere*, *19*(1), 206–234. https://doi.org/10.1130/GES02534.1

Blanco, J. F., Vargas, C. A., & Monsalve, G. (2017). Lithospheric thickness estimation beneath Northwestern South America from an *S*-wave receiver function analysis. *Geochemistry, Geophysics, Geosystems*, *18*(4), 1376–1387. https://doi.org/10.1002/2016GC006785

Boschman, L. M., van Hinsbergen, D. J. J., Torsvik, T. H., Spakman, W., & Pindell, J. L. (2014). Kinematic reconstruction of the Caribbean region since the Early Jurassic. *Earth-Science Reviews*, *138*, 102–136. https://doi.org/10.1016/j.earscirev.2014.08.007

Bourgois, J., Calle, B., Tournon, J., & Toussaint, J.-F. (1982). The Andean ophiolitic megastructures on the Buga-Buenaventura transverse (Western Cordillera—Valle Colombia). *Tectonophysics*, *18*(3–4), 207–229. https://doi.org/10.1016/0040-1951(82)90046-4

Braszus, B., Goes, S., Allen, R., Rietbrock, A., Collier, J., Harmon, N., et al. (2021). Subduction history of the Caribbean from upper-mantle seismic imaging and plate reconstruction. *Nature Communications*, *12*(1), 4211. https://doi.org/10.1038/s41467-021-24413-0

Brudzinski, M. R., Thurber, C. H., Hacker, B. R., & Engdahl, E. R. (2007). Global prevalence of double Benioff zones. *Science*, *316*(5830), 1472–1474. https://doi.org/10.1126/science.1139204

Buchs, D. M., Coombs, H., Irving, D., Wang, J., Koppers, A., Miranda, R., et al. (2019). Volcanic shutdown of the Panama Canal area following breakup of the Farallon plate. *Lithos*, *334–335*, 190–204. https://doi.org/10.1016/j.lithos.2019.02.016

Burdette, E., & Hirth, G. (2022). Creep rheology of antigorite: Experiments at subduction zone conditions. *Journal of Geophysical Research: Solid Earth*, *127*(7), e2022JB024260. https://doi.org/10.1029/2022JB024260

Burkett, E., & Gurnis, M. (2013). Stalled slab dynamics. *Lithosphere*, *5*(1), 92–97. https://doi.org/10.1130/L249.1

Cardona, A., León, S., Jaramillo, J. S., Montes, C., Valencia, V., Vanegas, J., et al. (2018). The Paleogene arcs of the northern Andes of Colombia and Panama: Insights on plate kinematic implications from new and existing geochemical, geochronological and isotopic data. *Tectonophysics*, *749*, 88–103. https://doi.org/10.1016/j.tecto.2018.10.032

Cardona, A., León, S., Jaramillo, J. S., Valencia, V. A., Zapata, S., Pardo-Trujillo, A., et al. (2020). Cretaceous record from a Mariana- to an Andean-type margin in the Central Cordillera of the Colombian Andes. In J. Gómez & A. O. Pinilla-Pachon (Eds.), *The geology of Colombia, volume 2 Mesozoic, Publicaciones Geológicas Especiales* (Vol. 36, pp. 335–373). Servicio Geológico Colombiano. https://doi.org/10.32685/pub.esp.36.2019.10

Carvajal-Arenas, L. C., & Mann, P. (2018). Western Caribbean intraplate deformation: Defining a continuous and active microplate boundary along the San Andres rift and Hess Escarpment fault zone, Colombian Caribbean Sea. *American Association of Petroleum Geologists Bulletin*, *102*(8), 1523–1563. https://doi.org/10.1306/12081717221

Cediel, F. & Shaw, R. P. (Eds.) (2019). Geology and tectonics of northwestern South America: The Pacific-Caribbean-Andean junction, *Frontiers in earth sciences*. Springer International Publishing. https://doi.org/10.1007/978-3-319-76132-9

Cediel, F., Shaw, R. P., & Cáceres, C. (2003). Tectonic assembly of the northern Andean block. In C. Bartolini, R. T. Buffler, & J. F. Blickwede (Eds.), *The circum-Gulf of Mexico and the Caribbean: Hydrocarbon habitats, Basin formation and plate tectonics, American Association of petroleum geologists memoir* (Vol. 79, pp. 815–848). The American Association of Petroleum Geologists. https://doi.org/10.1306/M79877C37

Chang, Y., Warren, L. M., & Prieto, G. A. (2017). Precise locations for intermediate-depth earthquakes in the Cauca cluster, Colombia. *Bulletin of the Seismological Society of America*, *107*(6), 2649–2663. https://doi.org/10.1785/0120170127

Chang, Y., Warren, L. M., Zhu, L., & Prieto, G. A. (2019). Earthquake focal mechanisms and stress field for the intermediate-depth Cauca cluster, Colombia. *Journal of Geophysical Research: Solid Earth*, *124*(1), 822–836. https://doi.org/10.1029/2018JB016804

Chatterjee, S. N., Pitt, A. M., & Iyer, H. M. (1985). Vp/Vs ratios in the Yellowstone National Park region, Wyoming. *Journal of Volcanology and Geothermal Research*, *26*(3–4), 213–230. https://doi.org/10.1016/0377-0273(85)90057-5

Chernak, L. J., & Hirth, G. (2010). Deformation of antigorite serpentinite at high temperature and pressure. *Earth and Planetary Science Letters*, *296*(1–2), 23–33. https://doi.org/10.1016/j.epsl.2010.04.035

Chiu, J.-M., Chiu, S.-C. C., & Kim, S. G. (1997). The significance of the crustal velocity model in local earthquake locations from a case example of a PANDA experiment in the central United States. *Bulletin of the Seismological Society of America*, *87*(6), 1537–1552. https://doi.org/10.1785/BSSA0870061537

Cochrane, R., Spikings, R., Gerdes, A., Winkler, W., Ulianov, A., Mora, A., & Chiaradia, M. (2014). Distinguishing between in-situ and accretionary growth of continents along active margins. *Lithos*, *202–203*, 382–394. https://doi.org/10.1016/j.lithos.2014.05.031

Codillo, E. A., Le Roux, V., & Marschall, H. R. (2018). Arc-like magmas generated by mélange-peridotite interaction in the mantle wedge. *Nature Communications*, *9*(1), 2864. https://doi.org/10.1038/s41467-018-05313-2

Colmenares, F., Román García, L., Sánchez, J. M., & Ramirez, J. C. (2019). Diagnostic structural features of NW South America: Structural cross sections based upon detailed field transects. In F. Cediel & R. P. Shaw (Eds.), *Geology and tectonics of northwestern South America, frontiers in Earth sciences* (pp. 651–672). Springer. https://doi.org/10.1007/978-3-319-76132-9_9

Comte, D., Dorbath, L., Pardo, M., Monfret, T., Haessler, H., Rivera, L., et al. (1999). A double-layered seismic zone in Arica, northern Chile. *Geophysical Research Letters*, *26*(13), 1965–1968. https://doi.org/10.1029/1999GL900447

Cordell, D., Unsworth, M. J., Diaz, D., Reyes-Wagner, V., Currie, C. A., & Hicks, S. P. (2019). Fluid and melt pathways in the Central Chilean subduction zone near the 2010 Maule earthquake (35-36°S) as inferred from magnetotelluric data. *Geochemistry, Geophysics, Geosystems*, *20*(4), 1818–1835. https://doi.org/10.1029/2018GC008167

Cortés, M., & Angelier, J. (2005). Current states of stress in the northern Andes as indicated by focal mechanisms of earthquakes. *Tectonophysics*, *403*(1–4), 29–58. https://doi.org/10.1016/j.tecto.2005.03.020

Cruz-Uribe, A. M., Marschall, H. R., Gaetani, G. A., & Le Roux, V. (2018). Generation of alkaline magmas in subduction zones by partial melting of mélange diapirs—An experimental study. *Geology*, *46*(4), 343–346. https://doi.org/10.1130/G39956.1

Dahm, T. (2000). Numerical simulations of the propagation path and the arrest of fluid-filled fractures in the Earth. *Geophysical Journal International*, *141*(3), 623–638. https://doi.org/10.1046/j.1365-246x.2000.00102.x

Daines, M. J., & Pec, M. (2015). Migration of melt. In H. Sigurdsson, B. Houghton, S. R. McNutt, H. Rymer, & J. Stix (Eds.), *The encyclopedia of volcanoes* (2nd ed., pp. 49–64). Elsevier. https://doi.org/10.1016/B978-0-12-385938-9.00002-X

Davey, F. J., & Ristau, J. (2011). Fore-arc mantle wedge seismicity under northeast New Zealand. *Tectonophysics*, *509*(3–4), 272–279. https://doi.org/10.1016/j.tecto.2011.06.017

Davies, J. H. (1999). The role of hydraulic fractures and intermediate-depth earthquakes in generating subduction-zone magmatism. *Nature*, *398*(6723), 142–145. https://doi.org/10.1038/18202

Deseta, N., Andersen, T. B., & Ashwal, L. D. (2014). A weakening mechanism for intermediate-depth seismicity? Detailed petrographic and microtextural observations from blueschist facies pseudotachylytes, Cape Corse, Corsica. *Tectonophysics*, *610*, 138–149. https://doi.org/10.1016/j.tecto.2013.11.007

Dickinson, W. R. (2009). Anatomy and global context of the North American Cordillera. In S. M. Kay, V. A. Ramos, & W. R. Dickinson (Eds.), *Backbone of the Americas: Shallow subduction, plateau uplift, and ridge and terrane collision, Geological Society of America Memoir* (Vol. 204, pp. 1–29). Geological Society of America. https://doi.org/10.1130/2009.1204(01)

Dilek, Y., & Sandvol, E. (2009). Seismic structure, crustal architecture and tectonic evolution of the Anatolian-African plate boundary and the Cenozoic orogenic belts in the Eastern Mediterranean region. In J. B. Murphy, J. D. Keppie, & A. J. Hynes (Eds.), *Ancient orogens and modern analogues, geological society of London special publication* (Vol. 327(1), pp. 127–160). Geological Society of London. https://doi.org/10.1144/SP327.8

Dixon, J. E., Dixon, T. H., Bell, D. R., & Malservisi, R. (2004). Lateral variation in upper mantle viscosity: Role of water. *Earth and Planetary Science Letters*, *222*(2), 451–467. https://doi.org/10.1016/j.epsl.2004.03.022

Dorbath, C., Gerbault, M., Carlier, G., & Guiraud, M. (2008). Double seismic zone of the Nazca plate in northern Chile: High-resolution velocity structure, petrological implications, and thermomechanical modeling. *Geochemistry, Geophysics, Geosystems*, *9*(7), Q07006. https://doi.org/10.1029/2008GC002020

Dougherty, S. L., Jiang, C., Clayton, R. W., Schmandt, B., & Hansen, S. M. (2021). Seismic evidence for a fossil slab origin for the Isabella anomaly. *Geophysical Journal International*, *224*(2), 1188–1196. https://doi.org/10.1093/gji/ggaa472

Duque-Caro, H. (1990). The Choco block in the northwestern corner of South America: Structural, tectonostratigraphic, and paleogeographic implications. *Journal of South American Earth Sciences*, *3*(1), 71–84. https://doi.org/10.1016/0895-9811(90)90019-W

Echeverri, S., Cardona, A., Pardo, A., Monsalve, G., Valencia, V. A., Borrero, C., et al. (2015). Regional provenance from southwestern Colombia fore-arc and intra-arc basins: Implications for middle to late Miocene orogeny in the northern Andes. *Terra Nova*, *27*(5), 356–363. https://doi.org/10.1111/ter.12167

Ego, F., Sébrier, M., & Yepes, H. (1995). Is the Cauca-Patia and Romeral Fault System left or rightlateral. *Geophysical Research Letters*, *22*(1), 33–36. https://doi.org/10.1029/94GL02837

Errázuriz-Henao, C., Gómez-Tuena, A., Duque-Trujillo, J., & Weber, M. (2019). The role of subducted sediments in the formation of intermediate mantle-derived magmas from the northern Colombian Andes. *Lithos*, *336–337*, 151–168. https://doi.org/10.1016/j.lithos.2019.04.007

Errázuriz-Henao, C., Gómez-Tuena, A., Parolari, M., & Weber, M. (2021). A biogeochemical imprint of the Panama Basin in the North Andean Arc. *Geochemistry, Geophysics, Geosystems*, *22*(7), e2021GC009835. https://doi.org/10.1029/2021GC009835

Ferrand, T. P., Hilairet, N., Incel, S., Deldicque, D., Labrousse, L., Gasc, J., et al. (2017). Dehydration-driven stress transfer triggers intermediate-depth earthquakes. *Nature Communications*, *8*(1), 15247. https://doi.org/10.1038/ncomms15247

Florez, M. A., & Prieto, G. A. (2019). Controlling factors of seismicity and geometry in double seismic zones. *Geophysical Research Letters*, *46*(8), 4174–4181. https://doi.org/10.1029/2018GL081168

French, M. E., Hirth, G., & Okazaki, K. (2019). Fracture-induced pore fluid pressure weakening and dehydration of serpentinite. *Tectonophysics*, *767*, 228168. https://doi.org/10.1016/j.tecto.2019.228168

Frohlich, C. (2006). *Deep earthquakes*. Cambridge University Press. https://doi.org/10.1017/CBO9781107297562

Fujii, N., Osamura, K., & Takahashi, E. (1986). Effect of water saturation on the distribution of partial melt in the olivine-pyroxene-plagioclase system. *Journal of Geophysical Research: Solid Earth*, *91*(B9), 9253–9259. https://doi.org/10.1029/JB091iB09p09253

Gasc, J., Hilairet, N., Yu, T., Ferrand, T., Schubnel, A., & Wang, Y. (2017). Faulting of natural serpentinite: Implications for intermediate-depth seismicity. *Earth and Planetary Science Letters*, *474*, 138–147. https://doi.org/10.1016/j.epsl.2017.06.016

George, S. W. M., Horton, B. K., Vallejo, C., Jackson, L. J., & Gutierrez, E. G. (2021). Did accretion of the Caribbean oceanic plateau drive rapid crustal thickening in the northern Andes? *Geology*, *49*(8), 936–940. https://doi.org/10.1130/G48509.1

Ghosh, D., Maiti, G., Mandal, N., & Baruah, A. (2020). Cold plumes initiated by Rayleigh-Taylor instabilities in subduction zones, and their characteristic volcanic distributions: The role of slab dip. *Journal of Geophysical Research: Solid Earth*, *125*(8), e2020JB019814. https://doi.org/10.1029/2020JB019814

Global Volcanism Program. (2024). Volcanoes of the world (v. 5.1.6; 2 Mar 2024). [Database]. *Distributed by Smithsonian Institution. compiled by Venzke, E.* Retrieved from https://volcano.si.edu/gvp_votw.cfm
Gomberg, J. S., Shedlock, K. M., & Roecker, S. W. (1990). The effect of *S*-wave arrival times on the accuracy of hypocenter estimation. *Bulletin of the Seismological Society of America*, *80*(6A), 1605–1628. https://doi.org/10.1785/BSSA08006A1605
González, R., Oncken, O., Faccenna, C., Le Breton, E., Bezada, M., & Mora, A. (2023). Kinematics and convergent tectonics of the northwestern South American plate during the Cenozoic. *Geochemistry, Geophysics, Geosystemts*, *24*(7), e2022GC010827. https://doi.org/10.1029/2022GC010827
Goswami, A., & Barbot, S. (2018). Slow-slip events in semi-brittle serpentinite fault zones. *Scientific Reports*, *8*(1), 6181. https://doi.org/10.1038/s41598-018-24637-z
Gutscher, M.-A., Malavieille, J., Lallemand, S., & Collot, J.-Y. (1999). Tectonic segmentation of the North Andean margin: Impact of the Carnegie Ridge collision. *Earth and Planetary Science Letters*, *168*(3–4), 255–270. https://doi.org/10.1016/S0012-821X(99)00060-6
Hack, A. C., & Thompson, A. B. (2011). Density and viscosity of hydrous magmas and related fluids and their role in subduction zone processes. *Journal of Petrology*, *52*(7–8), 1333–1362. https://doi.org/10.1093/petrology/egq048
Hacker, B. R., & Abers, G. A. (2012). Subduction factory 5: Unusually low Poisson's ratios in subduction zones from elastic anisotropy of peridotite. *Journal of Geophysical Research: Solid Earth*, *117*(B6), B06308. https://doi.org/10.1029/2012JB009187
Hacker, B. R., Abers, G. A., & Peacock, S. M. (2003). Subduction factory 1. Theoretical mineralogy, densities, seismic wave speeds, and H_2O contents. *Journal of Geophysical Research: Solid Earth*, *108*(B1), 2029. https://doi.org/10.1029/2001JB001127
Hacker, B. R., Gerya, T. V., & Gilotti, J. A. (2013). Formation and exhumation of ultrahigh-pressure terranes. *Elements*, *9*(4), 289–293. https://doi.org/10.2113/gselements.9.4.289
Hacker, B. R., Peacock, S. M., Abers, G. A., & Holloway, S. D. (2003). Subduction factory 2. Are intermediate-depth earthquakes in subducting slabs linked to metamorphic dehydration reactions? *Journal of Geophysical Research: Solid Earth*, *108*(B1), 2030. https://doi.org/10.1029/2001JB001129
Halpaap, F., Rondenay, S., Liu, Q., Millet, F., & Ottemöller, L. (2021). Toward waveform-based characterization of slab & mantle wedge (SAM) earthquakes. *Journal of Geophysical Research: Solid Earth*, *126*(9), e2020JB021573. https://doi.org/10.1029/2020JB021573
Halpaap, F., Rondenay, S., Perrin, A., Goes, S., Ottemöller, L., Austrheim, H., et al. (2019). Earthquakes track subduction fluids from slab source to mantle wedge sink. *Science Advances*, *5*(4), eaav7369. https://doi.org/10.1126/sciadv.aav7369
Hamza, V. M., Silva Dias, F. J. S., Gomes, A. J. L., & Delgadilho Terceros, Z. G. (2005). Numerical and functional representations of regional heat flow in South America. *Physics of the Earth and Planetary Interiors*, *152*(4), 223–256. https://doi.org/10.1016/j.pepi.2005.04.009
Hansen, L. N., & Warren, J. M. (2015). Quantifying the effect of pyroxene on deformation of peridotite in a natural shear zone. *Journal of Geophysical Research: Solid Earth*, *120*(4), 2717–2738. https://doi.org/10.1002/2014JB011584
Hao, M., Zhang, J. S., Pierotti, C. E., Zhou, W.-Y., Zhang, D., & Dera, P. (2020). The seismically fastest chemical heterogeneity in the Earth's deep upper mantle—Implications from the single-crystal thermoelastic properties of jadeite. *Earth and Planetary Science Letters*, *543*, 116345. https://doi.org/10.1016/j.epsl.2020.116345
Harlow, G. E., & Sorensen, S. S. (2005). Jade (nephrite and jadeitite) and serpentinite: Metasomatic connections. *International Geology Review*, *47*(2), 113–146. https://doi.org/10.2747/0020-6814.47.2.113
Harlow, G. E., Tsujimori, T., & Sorensen, S. S. (2015). Jadeitites and plate tectonics. *Annual Review of Earth and Planetary Sciences*, *43*(1), 105–138. https://doi.org/10.1146/annurev-earth-060614-105215
Hayes, G. P., Moore, G. L., Portner, D. E., Hearne, M., Flamme, H., Furtney, M., & Smoczyk, G. M. (2018). Slab2, a comprehensive subduction zone geometry model. *Science*, *362*(6410), 58–61. https://doi.org/10.1126/science.aat4723
Hilairet, N., Reynard, B., Wang, Y., Daniel, I., Merkel, S., Nishiyama, N., & Petitgirard, S. (2007). High-pressure creep of serpentine, interseismic deformation, and initiation of subduction. *Science*, *318*(5858), 1910–1913. https://doi.org/10.1126/science.1148494
Hobbs, B. E., & Ord, A. (1988). Plastic instabilities: Implications for the origin of intermediate and deep focus earthquakes. *Journal of Geophysical Research: Solid Earth*, *93*(B9), 10521–10540. https://doi.org/10.1029/JB093iB09p10521
Holness, M. B. (1997). Surface chemical controls on pore-fluid connectivity in texturally equilibrated materials. In B. Jamtveit & B. W. D. Yardley (Eds.), *Fluid flow and transport in rocks* (pp. 149–169). Springer. https://doi.org/10.1007/978-94-009-1533-6_9
Huang, Y., Nakatani, T., Nakamura, M., & McCammon, C. (2020). Experimental constraint on grain-scale fluid connectivity in subduction zones. *Earth and Planetary Science Letters*, *552*, 116610. https://doi.org/10.1016/j.epsl.2020.116610
Huesca-Pérez, E., Gutierrez-Reyes, E., Valenzuela, R. W., Husker, A., & Mayer, S. (2021). 3-D travel-time tomography of southernmost Baja California Peninsula. *Journal of South American Earth Sciences*, *105*, 102966. https://doi.org/10.1016/j.jsames.2020.102966
Hughes, G. R., & Mahood, G. A. (2008). Tectonic controls on the nature of large silicic calderas in volcanic arcs. *Geology*, *36*(8), 627–630. https://doi.org/10.1130/G24796A.1
Idárraga-García, J., Kendall, J.-M., & Vargas, C. A. (2016). Shear wave anisotropy in northwestern South America and its link to the Caribbean and Nazca subduction geodynamics. *Geochemistry, Geophysics, Geosystems*, *17*(9), 3655–3673. https://doi.org/10.1002/2016GC006323
International Seismological Centre. (2024). On-line bulletin. https://doi.org/10.31905/D808B830
Ismail-Zadeh, A., Matenco, L., Radulian, M., Cloetingh, S., & Panza, G. (2012). Geodynamics and intermediate-depth seismicity in Vrancea (the south-eastern Carpathians): Current state-of-the art. *Tectonophysics*, *530–531*, 50–79. https://doi.org/10.1016/j.tecto.2012.01.016
Jaillard, E. (2022). Late Cretaceous-Paleogene orogenic build-up of the Ecuadorian Andes: Review and discussion. *Earth-Science Reviews*, *230*, 104033. https://doi.org/10.1016/j.earscirev.2022.104033
Jaramillo, J. S., Cardona, A., León, S., Valencia, V., & Vinasco, C. (2017). Geochemistry and geochronology from Cretaceous magmatic and sedimentary rocks at 6°35′ N, western flank of the Central Cordillera (Colombian Andes): Magmatic record of arc growth and collision. *Journal of South American Earth Sciences*, *76*, 460–481. https://doi.org/10.1016/j.jsames.2017.04.012
Jarrin, P., Nocquet, J.-M., Rolandone, F., Audin, L., Mora-Páez, H., Alvarado, A., et al. (2023). Continental block motion in the Northern Andes from GPS measurements. *Geophysical Journal International*, *235*(2), 1434–1464. https://doi.org/10.1093/gji/ggad294
Ji, Y., Yoshioka, S., Manea, V. C., & Manea, M. (2017). Seismogenesis of dual subduction beneath Kanto, central Japan controlled by fluid release. *Scientific Reports*, *7*(1), 16864. https://doi.org/10.1038/s41598-017-16818-z
Jiang, C., Schmandt, B., Hansen, S. M., Dougherty, S. L., Clayton, R. W., Farrell, J., & Lin, F.-C. (2018). Rayleigh and S wave tomography constraints on subduction termination and lithospheric foundering in central California. *Earth and Planetary Science Letters*, *488*, 14–26. https://doi.org/10.1016/j.epsl.2018.02.009
John, T., Medvedev, S., Rüpke, L. H., Andersen, T. B., Podladchikov, Y. Y., & Austrheim, H. (2009). Generation of intermediate-depth earthquakes by self-localizing thermal runaway. *Nature Geoscience*, *2*, 137–140. https://doi.org/10.1038/ngeo419

Jung, H., & Green, H. W., II. (2004). Experimental faulting of serpentinite during dehydration: Implications for earthquakes, seismic low-velocity zones, and anomalous hypocenter distributions in subduction zones. *International Geology Review*, *46*(12), 1089–1102. https://doi.org/10.2747/0020-6814.46.12.1089

Kapp, P., & DeCelles, P. G. (2019). Mesozoic-Cenozoic geological evolution of the Himalayan-Tibetan Orogen and working tectonic hypotheses. *American Journal of Science*, *319*(3), 159–254. https://doi.org/10.2475/03.2019.01

Kelemen, P. B., & Hirth, G. (2007). A periodic shear-heating mechanism for intermediate-depth earthquakes in the mantle. *Nature*, *446*(7137), 787–790. https://doi.org/10.1038/nature05717

Kelemen, P. B., Hirth, G., Shimizu, N., Spiegelman, M., & Dick, H. J. (1997). A review of melt migration processes in the adiabatically upwelling mantle beneath oceanic spreading ridges. *Philosophical Transactions of the Royal Society A*, *355*(1723), 283–318. https://doi.org/10.1098/rsta.1997.0010

Kellogg, J. N., Franco Camelio, G. B., & Mora-Páez, H. M. (2019). Cenozoic tectonic evolution of the North Andes with constraints from volcanic ages, seismic reflection, and satellite geodesy. In B. K. Horton & A. Folguera (Eds.), *Andean tectonics* (pp. 69–102). Elsevier. https://doi.org/10.1016/B978-0-12-816009-1.00006-X

Kellogg, J. N., Vega, V., Stailings, T. C., & Aiken, C. L. (1995). Tectonic development of Panama, Costa Rica, and the Colombian Andes: Constraints from global positioning system geodetic studies and gravity. In P. Mann (Ed.), *Geologic and tectonic development of the Caribbean Plate boundary in southern Central America, geological society of America special paper* (Vol. 295, pp. 75–90). Geological Society of America. https://doi.org/10.1130/SPE295-p75

Kita, S., & Ferrand, T. P. (2018). Physical mechanisms of oceanic mantle earthquakes: Comparison of natural and experimental events. *Scientific Reports*, *8*(1), 17049. https://doi.org/10.1038/s41598-018-35290-x

Klein, B. Z., & Behn, M. D. (2021). On the evolution and fate of sediment diapirs in subduction zones. *Geochemistry, Geophysics, Geosystems*, *22*(11), e2021GC009873. https://doi.org/10.1029/2021GC009873

Kohlstedt, D. L., & Holtzman, B. K. (2009). Shearing melt out of the Earth: An experimentalist's perspective on the influence of deformation on melt extraction. *Annual Review of Earth and Planetary Sciences*, *37*(1), 561–593. https://doi.org/10.1146/annurev.earth.031208.100104

Kufner, S.-K., Kakar, N., Bezada, M., Bloch, W., Metzger, S., Yuan, X., et al. (2021). The Hindu Kush slab break-off as revealed by deep structure and crustal deformation. *Nature Communications*, *12*(1), 1685. https://doi.org/10.1038/s41467-021-21760-w

Laigle, M., Hirn, A., Sapin, M., Bécel, A., Charvis, P., Flueh, E., et al. (2013). Seismic structure and activity of the north-central Lesser Antilles subduction zone from an integrated approach: Similarities with the Tohoku forearc. *Tectonophysics*, *603*, 1–20. https://doi.org/10.1016/j.tecto.2013.05.043

Lakey, S., & Hermann, J. (2022). An experimental study of chlorite stability in varied subduction zone lithologies with implications for fluid production, melting, and diapirism in chlorite-rich mélange rocks. *Journal of Petrology*, *63*(4), 1–29. https://doi.org/10.1093/petrology/egac029

Lara, M., Salazar-Franco, A. M., & Silva-Tamayo, J. C. (2018). Provenance of the Cenozoic siliciclastic intramontane Amagá formation: Implications for the early Miocene collision between Central and South America. *Sedimentary Geology*, *373*, 147–162. https://doi.org/10.1016/j.sedgeo.2018.06.003

Leal-Mejía, H., Shaw, R. P., & Melgarejo i Draper, J. C. (2019). Spatial-temporal migration of granitoid magmatism and the Phanerozoic tectono-magmatic evolution of the Colombian Andes. In F. Cediel & R. P. Shaw (Eds.), *Geology and tectonics of northwestern South America, frontiers in Earth sciences* (pp. 253–410). Springer. https://doi.org/10.1007/978-3-319-76132-9_5

León, S., Cardona, A., Parra, M., Sobel, E. R., Jaramillo, J. S., Glodny, J., et al. (2018). Transition from collisional to subduction-related regimes: An example from Neogene Panama-Nazca-South America interactions. *Tectonics*, *37*(1), 119–139. https://doi.org/10.1002/2017TC004785

Lin, G., & Shearer, P. M. (2009). Evidence for water-filled cracks in earthquake source regions. *Geophysical Research Letters*, *36*(17), L17315. https://doi.org/10.1029/2009GL039098

Linkimer, L., Beck, S., Zandt, G., Alvarado, P., Anderson, M., Gilbert, H., & Zhang, H. (2020). Lithospheric structure of the Pampean flat slab region from double-difference tomography. *Journal of South American Earth Sciences*, *97*, 102417. https://doi.org/10.1016/j.jsames.2019.102417

Linkimer, L., Beck, S. L., Schwartz, S. Y., Zandt, G., & Levin, V. (2010). Nature of crustal terranes and the Moho in northern Costa Rica from receiver function analysis. *Geochemistry, Geophysics, Geosystems*, *11*(1), Q01S19. https://doi.org/10.1029/2009GC002795

Lister, G., Kennett, B., Richards, S., & Forster, M. (2008). Boudinage of a stretching slablet implicated in earthquakes beneath the Hindu Kush. *Nature Geoscience*, *1*(3), 196–201. https://doi.org/10.1038/ngeo132

Londoño, J. M. (2016). Evidence of recent deep magmatic activity at Cerro Bravo-Cerro Machín volcanic complex, central Colombia. Implications for future volcanic activity at Nevado del Ruiz, Cerro Manchín and other volcanoes. *Journal of Volcanology and Geothermal Research*, *324*, 156–168. https://doi.org/10.1016/j.jvolgeores.2016.06.003

Londoño, J. M., & Kumagai, H. (2018). 4D seismic tomograrphy of Nevado del Ruiz volcano, Colombia, 2000-2016. *Journal of Volcanology and Geothermal Research*, *358*, 105–123. https://doi.org/10.1016/j.jvolgeores.2018.02.015

Londoño, J. M., Quintero, S., Vallejo, K., Muñoz, F., & Romero, J. (2019). Seismicity of Valle Medio del Magdalena basin, Colombia. *Journal of South American Earth Sciences*, *92*, 565–585. https://doi.org/10.1016/j.jsames.2019.04.003

Lonsdale, P. (2005). Creation of the Cocos and Nazca plates by fission of the Farallon plate. *Tectonophysics*, *404*(3–4), 237–264. https://doi.org/10.1016/j.tecto.2005.05.011

Lu, P., Zhang, H., Gao, L., & Comte, D. (2021). Seismic imaging of the double seismic zone in the subducting slab in northern Chile. *Earthquake Research Advances*, *1*(1), 100003. https://doi.org/10.1016/j.eqrea.2021.100003

Madella, A., & Ehlers, T. A. (2021). Contribution of background seismicity to forearc uplift. *Nature Geoscience*, *14*(8), 620–625. https://doi.org/10.1038/s41561-021-00779-0

Manning, C. E. (2004). The chemistry of subduction-zone fluids. *Earth and Planetary Science Letters*, *223*(1–2), 1–16. https://doi.org/10.1016/j.epsl.2004.04.030

Manning, C. E., & Frezzotti, M. L. (2020). Subduction-zone fluids. *Elements*, *16*(6), 395–400. https://doi.org/10.2138/gselements.16.6.395

Manthilake, G., Chantel, J., Guignot, N., & King, A. (2021). The anomalous seismic behavior of aqueous fluids released during dehydration of chlorite in subduction zones. *Minerals*, *11*(1), 70. https://doi.org/10.3390/min11010070

Marín-Cerón, M. I., Leal-Mejía, H., Bernet, M., & Mesa-García, J. (2019). Late Cenozoid to modern-day volcanism in the northern Andes: A geochronological, petrographical, and geochemical review. In F. Cediel & R. P. Shaw (Eds.), *Geology and tectonics of northwestern South America, frontiers in Earth sciences* (pp. 603–648). Springer. https://doi.org/10.1007/978-3-319-76132-9_8

Marot, M., Monfret, T., Pardo, M., Ranalli, G., & Nolet, G. (2013). A double seismic zone in the subducting Juan Fernandez ridge of the Nazca Plate (32°S), central Chile. *Journal of Geophysical Research: Solid Earth*, *118*(7), 3462–3475. https://doi.org/10.1002/jgrb.50240

Marschall, H. R., & Schumacher, J. C. (2012). Arc magmas sourced from mélange diapirs in subduction zones. *Nature Geoscience*, *5*(12), 862–867. https://doi.org/10.1038/ngeo1634

Martínez-Jaramillo, D., & Prieto, G. A. (2024). Tectonic setting of the northwestern Andes constrained by a high-resolution earthquake catalog: Block kinematics. *Journal of South American Earth Sciences*, *134*, 104761. https://doi.org/10.1016/j.jsames.2023.104761

McKenzie, D. (1984). The generation and compaction of partially molten rock. *Journal of Petrology*, *25*(3), 713–765. https://doi.org/10.1093/petrology/25.3.713

Meschede, M., & Barckhausen, U. (2000). Plate tectonic evolution of the Cocos-Nazca spreading center. In E. A. Silver, G. Kimura, & T. H. Shipley (Eds.), *Proceedings of the oceanic drilling program, scientific results* (Vol. 170, pp. 1–10). Ocean Drilling Program. https://doi.org/10.2973/odp.proc.sr.170.009.2000

Meyer, R. P., Mooney, W. D., Hales, A. L., Helsley, C. E., Woollard, G. P., Hussong, D. M., et al. (1976). Project Nariño III: Refraction observation across a leading edge, Malpelo island to the Colombian Cordillera occidental. In G. H. Sutton, M. H. Manghnani, R. Moberly, & E. U. Mcafee (Eds.), *The geophysics of the Pacific Ocean Basin and its margin, geophysical monograph* (Vol. 19, pp. 105–132). American Geophysical Union. https://doi.org/10.1029/GM019p0105

Mibe, K., Yoshino, T., Ono, S., Yasuda, A., & Fujii, T. (2003). Connectivity of aqueous fluid in eclogite and its implications for fluid migration in the Earth's interior. *Journal of Geophysical Research*, *108*(B6), 2295. https://doi.org/10.1029/2002JB001960

Miller, N. C., & Behn, M. D. (2012). Timescales for the growth of sediment diapirs in subduction zones. *Geophysical Journal International*, *190*(3), 1361–1377. https://doi.org/10.1111/j.1365-246X.2012.05565.x

Mirwald, A., Cruz-Atienza, V. M., Díaz-Mojica, J., Iglesias, A., Singh, S. K., Villafuerte, C., & Tago, J. (2019). The 19 September 2017 (M_W 7.1) intermediate-depth Mexican earthquake: A slow and energetically inefficient deadly shock. *Geophysical Research Letters*, *46*(4), 2054–2064. https://doi.org/10.1029/2018GL080904

Mojica Boada, M. J., Poveda, E., & Tary, J. B. (2022). Lithospheric and slab configurations from receiver function imaging in northwestern South America, Colombia. *Journal of Geophysical Research: Solid Earth*, *127*(12), e2022JB024475. https://doi.org/10.1029/2022JB024475

Montes, C., Bayona, G., Cardona, A., Buchs, D. M., Silva, C. A., Morón, S., et al. (2012). Arc-continent collision and orocline formation: Closing of the Central American seaway. *Journal of Geophysical Research*, *117*(B4), B04105. https://doi.org/10.1029/2011JB008959

Montes, C., Hatcher, R. D., Jr., & Restrepo-Pace, P. A. (2005). Tectonic reconstruction of the northern Andean blocks: Oblique convergence and rotations derived from the kinematics of the Piedras-Girardot area, Colombia. *Tectonophysics*, *399*(1–4), 221–250. https://doi.org/10.1016/j.tecto.2004.12.024

Montes, C., Rodriguez-Corcho, A. F., Bayona, G., Hoyos, N., Zapata, S., & Cardona, A. (2019). Continental margin response to multiple arc-continent collisions: The northern Andes-Caribbean margin. *Earth-Science Reviews*, *198*, 102903. https://doi.org/10.1016/j.earscirev.2019.102903

Mora-Bohórquez, J. A., Ibánez-Mejia, M., Oncken, O., de Freitas, M., Vélez, V., Mesa, A., & Serna, L. (2017). Structure and age of the Lower Magdalena Valley basin basement, northern Colombia: New reflection-seismic and U-Pb-Hf insights into the termination of the central Andes against the Caribbean basin. *Journal of South American Earth Sciences*, *74*, 1–26. https://doi.org/10.1016/j.jsames.2017.01.001

Mora-Páez, H., Mencin, D. J., Molnar, P., Diederix, H., Cardona-Piedrahita, L., Peláez-Gaviria, J.-R., & Corchuelo-Cuervo, Y. (2016). GPS velocities and the construction of the Eastern Cordillera of the Colombian Andes. *Geophysical Research Letters*, *43*(16), 8407–8416. https://doi.org/10.1002/2016GL069795

Nakajima, J., & Uchida, N. (2018). Repeated drainage from megathrusts during episodic slow slip. *Nature Geoscience*, *11*(5), 351–356. https://doi.org/10.1038/s41561-018-0090-z

Nakata, K., Kobayashi, A., Katsumata, A., Hirose, F., Nishimiya, T., Kimura, K., et al. (2019). Double seismic zone and seismicity in the mantle wedge beneath the Ogasawara Islands identified by an ocean bottom seismometer observation. *Earth Planets and Space*, *71*(1), 29. https://doi.org/10.1186/s40623-019-1012-z

Nicholson, C., Sorlien, C. C., Atwater, T., Crowell, J. C., & Luyendyk, B. P. (1994). Microplate capture, rotation of the western Transverse Ranges, and initiation of the San Andreas transform as a low-angle fault system. *Geology*, *22*(6), 491–495. https://doi.org/10.1130/0091-7613(1994)022<0491:MCROTW>2.3.CO;2

Nicolas, A. (1986). A melt extraction model based on structural studies in mantle peridotites. *Journal of Petrology*, *27*(4), 999–1022. https://doi.org/10.1093/petrology/27.4.999

Nielsen, S. G., & Marschall, H. R. (2017). Geochemical evidence for mélange melting in global arcs. *Science Advances*, *3*(4), e1602402. https://www.science.org/doi/10.1126/sciadv.1602402

Ogawa, M. (1987). Shear instability in viscoelastic material as the cause of deep focus earthquakes. *Journal of Geophysical Research: Solid Earth*, *92*(B13), 13801–13810. https://doi.org/10.1029/JB092iB13p13801

Ohuchi, T., Lei, X., Ohfuji, H., Higo, Y., Tange, Y., Sakai, T., et al. (2017). Intermediate-depth earthquakes linked to localized heating in dunite and harzburgite. *Nature Geoscience*, *10*, 771–776. https://doi.org/10.1038/ngeo3011

Ojeda, A., & Havskov, J. (2001). Crustal structure and local seismicity in Colombia. *Journal of Seismology*, *5*(4), 575–593. https://doi.org/10.1023/A:1012053206408

Okazaki, K., & Katayama, I. (2015). Slow stick slip of antigorite serpentinite under hydrothermal conditions as a possible mechanism for slow earthquakes. *Geophysical Research Letters*, *42*(4), 1099–1104. https://doi.org/10.1002/2014GL062735

Paulatto, M., Laigle, M., Galve, A., Charvis, P., Sapin, M., Bayrakci, G., et al. (2017). Dehydration of subducting slow-spread oceanic lithosphere in the Lesser Antilles. *Nature Communications*, *8*(1), 15980. https://doi.org/10.1038/ncomms15980

Paulssen, H., & de Vos, D. (2017). Slab remnants beneath the Baja California peninsula: Seismic constraints and tectonic implications. *Tectonophysics*, *719–720*, 27–36. https://doi.org/10.1016/j.tecto.2016.09.021

Peacock, S. M. (2001). Are the lower planes of double seismic zones caused by serpentine dehydration in subducting oceanic mantle? *Geology*, *29*(4), 299–302. https://doi.org/10.1130/0091-7613(2001)029<0299:ATLPOD>2.0.CO;2

Peacock, S. M., & Wang, K. (2021). On the stability of talc in subduction zones: A possible control on the maximum depth of decoupling between the subducting plate and mantle wedge. *Geophysical Research Letters*, *48*(17), e2021GL094889. https://doi.org/10.1029/2021GL094889

Pedraza, P., & Pulido, N. (2018). *Minimum 1D seismic velocity model from local earthquakes data in Servitá Fault System, Eastern Cordillera of Colombia*. Servicio Geológico Colombiano.

Peng, Y., Mookherjee, M., Hermann, A., Manthilake, G., & Mainprice, D. (2022). Anomalous elasticity of talc at high pressures: Implications for subduction systems. *Geoscience Frontiers*, *13*(4), 101381. https://doi.org/10.1016/j.gsf.2022.101381

Pennington, W. D. (1981). Subduction of the eastern Panama Basin and seismotectonics of northwestern South America. *Journal of Geophysical Research*, *86*(B11), 10753–10770. https://doi.org/10.1029/JB086iB11p10753

Pérez-Consuegra, N., Ott, R. F., Hoke, G. D., Galve, J. P., Pérez-Peña, V., & Mora, A. (2021). Neogene variations in slab geometry drive topographic change and drainage reorganization in the Northern Andes of Colombia. *Global and Planetary Change*, *206*, 103641. https://doi.org/10.1016/j.gloplacha.2021.103641

Piedrahita, V. A., Bernet, M., Chadima, M., Sierra, G. M., Marín-Cerón, M. I., & Toro, G. E. (2017). Detrital zircon fission-track thermochronology and magnetic fabric of the Amagá Formation (Colombia): Intracontinental deformation and exhumation events in the northwestern Andes. *Sedimentary Geology*, *356*, 26–42. https://doi.org/10.1016/j.sedgeo.2017.05.003

Pindell, J., Kennan, L., Maresch, W. V., Stanek, K.-P., Draper, G., & Higgs, R. (2005). Plate-kinematics and crustal dynamics of circum-Caribbean arc-continent interactions: Tectonic controls on basin development in Proto-Caribbean margins. In H. G. Avé Lallemant & V. B. Sisson (Eds.), *Caribbean-South American plate interactions, Venezuela, geological society of America special paper* (Vol. 394, pp. 7–52). Geological Society of America. https://doi.org/10.1130/0-8137-2394-9.7

Pindell, J. L., & Kennan, L. (2009). Tectonic evolution of the Gulf of Mexico, Caribbean and northern South America in the mantle reference frame: An update. In K. H. James, M. A. Lorente, & J. L. Pindell (Eds.), *The origin and evolution of the Caribbean Plate, geological society of London special publication* (Vol. 328, pp. 1–55). Geological Society of London. https://doi.org/10.1144/SP328.1

Poli, P., Prieto, G., Rivera, E., & Ruiz, S. (2016). Earthquakes initiation and thermal shear instability in the Hindu Kush intermediate depth nest. *Geophysical Research Letters*, *43*(4), 1537–1542. https://doi.org/10.1002/2015GL067529

Poli, P., Prieto, G. A., Yu, C. Q., Florez, M., Agurto-Detzel, H., Mikesell, T. D., et al. (2016). Complex rupture of the *M*6.3 2015 March 10 Bucaramanga earthquake: Evidence of strong weakening process. *Geophysical Journal International*, *205*(2), 988–994. https://doi.org/10.1093/gji/ggw065

Porritt, R. W., Becker, T. W., & Monsalve, G. (2014). Seismic anisotropy and slab dynamics from *SKS* splitting recorded in Colombia. *Geophysical Research Letters*, *41*(24), 8775–8783. https://doi.org/10.1002/2014GL061958

Poveda, E., Julià, J., Schimmel, M., & Perez-Garcia, N. (2018). Upper and middle crustal velocity structure of the Colombian Andes from ambient noise tomography: Investigating subduction-related magmatism in the overriding plate. *Journal of Geophysical Research: Solid Earth*, *123*(2), 1459–1485. https://doi.org/10.1002/2017JB014688

Poveda, E., Monsalve, G., & Vargas, C. A. (2015). Receiver functions and crustal structure of the northwestern Andean region, Colombia. *Journal of Geophysical Research: Solid Earth*, *120*(4), 2408–2425. https://doi.org/10.1002/2014JB011304

Prieto, G. A., Beroza, G. C., Barrett, S. A., López, G. A., & Florez, M. (2012). Earthquake nests as natural laboratories for the study of intermediate-depth earthquake mechanics. *Tectonophysics*, *570–571*, 42–56. https://doi.org/10.1016/j.tecto.2012.07.019

Prieto, G. A., Florez, M., Barrett, S. A., Beroza, G. C., Pedraza, P., Faustino Blanco, J., & Poveda, E. (2013). Seismic evidence for thermal runaway during intermediate-depth earthquake rupture. *Geophysical Research Letters*, *40*(23), 6064–6068. https://doi.org/10.1002/2013GL058109

Prieto, G. A., Forment, B., Yu, C., Poli, P., & Abercrombie, R. (2017). Earthquake rupture below the brittle-ductile transition in continental lithospheric mantle. *Science Advances*, *3*, e1602642. https://doi.org/10.1126/sciadv.1602642

Restrepo, J. J., & Toussaint, J. F. (2020). Tectonostratigraphic terranes in Colombia: An update. First part: Continental Terranes. In J. Gómez & D. Mateus-Zabala (Eds.), *The geology of Colombia, volume 1 Proterozoic – Paleozoic, Publicaciones Geológicas Especiales* (Vol. 35, pp. 37–63). Bogotá: Servicio Geológico Colombiano. https://doi.org/10.32685/pub.esp.35.2019.03

Reynard, B. (2013). Serpentine in active subduction zones. *Lithos*, *178*, 171–185. https://doi.org/10.1016/j.lithos.2012.10.012

Reynard, B., Mibe, K., & Van de Moortèle, B. (2011). Electrical conductivity of the serpentinised mantle and fluid flow in subduction zones. *Earth and Planetary Science Letters*, *307*(3–4), 387–394. https://doi.org/10.1016/j.epsl.2011.05.013

Richard, G., Monnereau, M., & Rabinowicz, M. (2007). Slab dehydration and fluid migration at the base of the upper mantle: Implications for deep earthquake mechanisms. *Geophysical Journal International*, *168*(3), 1291–1304. https://doi.org/10.1111/j.1365-246X.2006.03244.x

Rietbrock, A., & Waldhauser, F. (2004). A narrowly spaced double-seismic zone in the subducting Nazca plate. *Geophysical Research Letters*, *31*(10), L10608. https://doi.org/10.1029/2004GL019610

Robertson, A. H. F., Parlak, O., & Ustaömer, T. (2012). Overview of the Palaeozoic-Neogene evolution of Neotethys in the eastern Mediterranean region (southern Turkey, Cyprus, Syria). *Petroleum Geoscience*, *18*(4), 381–404. https://doi.org/10.1144/petgeo2011-091

Rodríguez, G., & Zapata, G. (2012). Características del plutonismo Mioceno superior en el segmento norte de la cordillera Occidental e implicaciones tectónicas en el modelo geológico del noroccidente colombiano. *Boletín de Ciencias de la Tierra* (31), 5–22.

Rodriguez-Corcho, A. F., Rojas-Agramonte, Y., Barrera-Gonzalez, J. A., Marroquin-Gomez, M. P., Bonilla-Correa, S., Izquierdo-Camacho, D., et al. (2022). The Colombian geochronological database (CGD). *International Geology Review*, *64*(12), 1635–1669. https://doi.org/10.1080/00206814.2021.1954556

Rosenbaum, G., Caulfield, J. T., Ubide, T., Ward, J. F., Sandiford, D., & Sandiford, M. (2021). Spatially and geochemically anomalous arc magmatism: Insights from the Andean arc. *Geochemistry, Geophysics, Geosystems*, *22*(6), e2021GC009688. https://doi.org/10.1029/2021GC009688

Ryan, W. B. F., Carbotte, S. M., Coplan, J. O., O'Hara, S., Melkonian, A., Arko, R., et al. (2009). Global multi-resolution topography synthesis. *Geochemistry, Geophysics, Geosystems*, *10*(3), Q03014. https://doi.org/10.1029/2008GC002332

Schmeling, H., Kruse, J. P., & Richard, G. (2012). Effective shear and bulk viscosity of partially molten rock based on elastic moduli theory of a fluid filled poroelastic medium. *Geophysical Journal International*, *190*(3), 1571–1578. https://doi.org/10.1111/j.1365-246X.2012.05596.x

Schurr, B., & Rietbrock, A. (2004). Deep seismic structure of the Atacama basin, northern Chile. *Geophysical Research Letters*, *31*(12), L12601. https://doi.org/10.1029/2004GL019796

Servicio Geológico Colombiano. (1993a). Catálogo de Sismicidad [Dataset]. *Servicio Geológico Colombiano*. Retrieved from https://bdrsnc.sgc.gov.co/paginas1/catalogo/index.php

Servicio Geológico Colombiano. (1993b). Red Sismologica Nacional de Colombia [Dataset]. *International Federation of Digital Seismograph Networks*. https://doi.org/10.7914/SN/CM

Servicio Geológico Colombiano. (2019a). Boletín extraordinario de actividad del volcán Nevado del Huila del 26 de enero de 2019. Retrieved from https://www2.sgc.gov.co/Noticias/boletinesDocumentos/Bolet%C3%ADn%20extraordinario%20de%20actividad%20del%20volc%C3%A1n%20Nevado%20del%20Huila%20del%2026%20de%20enero%20de%202019.pdf

Servicio Geológico Colombiano. (2019b). Boletín mensual de actividad volcánica segment central enero 2019. Retrieved from https://www2.sgc.gov.co/Noticias/boletinesDocumentos/Bolet%C3%ADn%20mensual%20de%20actividad%20volc%C3%A1nica%20segmento%20central%20enero%202019.pdf

Shearer, P. M. (1988). Cracked media, Poisson's ratio and the structure of the upper oceanic crust. *Geophysical Journal International*, *92*(2), 357–362. https://doi.org/10.1111/j.1365-246X.1988.tb01149.x

Sheldrake, T., Caricchi, L., & Scutari, M. (2020). Tectonic controls on global variations of large-magnitude explosive eruptions in volcanic arcs. *Frontiers in Earth Science*, *8*, 127. https://doi.org/10.3389/feart.2020.00127

Sippl, C., Schurr, B., Asch, G., & Kummerow, J. (2018). Seismicity structure of the northern Chile forearc from >100,000 double-difference relocated hypocenters. *Journal of Geophysical Research: Solid Earth*, *123*(5), 4063–4087. https://doi.org/10.1002/2017JB015384

Sippl, C., Schurr, B., John, T., & Hainzl, S. (2019). Filling the gap in a double seismic zone: Intraslab seismicity in northern Chile. *Lithos*, *346–347*, 105155. https://doi.org/10.1016/j.lithos.2019.105155

Somoza, R., & Ghidella, M. E. (2012). Late Cretaceous to recent plate motions in western South America revisited. *Earth and Planetary Science Letters*, *331–332*, 152–163. https://doi.org/10.1016/j.epsl.2012.03.003

Špičák, A., Hanuš, V., & Vaněk, J. (2004). Seismicity pattern: An indicator of source region of volcanism at convergent plate margins. *Physics of the Earth and Planetary Interiors*, *141*(4), 303–326. https://doi.org/10.1016/j.pepi.2003.11.005

Špičák, A., Vaněk, J., & Hanuš, V. (2009). Seismically active column and volcanic plumbing system beneath the island arc of the Izu-Bonin subduction zone. *Geophysical Journal International*, *179*(3), 1301–1312. https://doi.org/10.1111/j.1365-246X.2009.04375.x

Stern, R. J., & Scholl, D. W. (2010). Yin and yang of continental crust creation and destruction by plate tectonic processes. *International Geology Review*, *52*, 1–31. https://doi.org/10.1080/00206810903332322

Suárez-Rodríguez, M. A. (2007). Geological framework of the Pacific Coast sedimentary basins, western Colombia. *Geología Colombiana*, *32*, 47–62.

Sun, F., Li, Y., He, Q., Liu, L., Wang, Z., Xu, C., et al. (2022). Sound velocity anomalies of limestone at high pressure and implications for the mantle wedge. *High Pressure Research*, *42*(4), 336–348. https://doi.org/10.1080/08957959.2022.2145562

Sun, M., & Bezada, M. (2019). Seismogenic necking during slab detachment: Evidence from relocation of intermediate-depth seismicity in the Alboran slab. *Journal of Geophysical Research: Solid Earth*, *125*(2), e2019JB017896. https://doi.org/10.1029/2019JB017896

Sun, M., Bezada, M. J., Cornthwaite, J., Prieto, G. A., Niu, F., & Levander, A. (2022). Overlapping slabs: Untangling subduction in NW South America through finite-frequency teleseismic tomography. *Earth and Planetary Science Letters*, *577*, 117253. https://doi.org/10.1016/j.epsl.2021.117253

Suter, F., Sartori, M., Neuwerth, R., & Gorin, G. (2008). Structural imprints at the front of the Chocó-Panamá indenter: Field data from the North Cauca Valley Basin, central Colombia. *Tectonophysics*, *460*(1–4), 134–157. https://doi.org/10.1016/j.tecto.2008.07.015

Syracuse, E. M., Maceira, M., Prieto, G. A., Zhang, H., & Ammon, C. J. (2016). Multiple plates subducting beneath Colombia, as illuminated by seismicity and velocity from the joint inversion of seismic and gravity data. *Earth and Planetary Science Letters*, *444*, 139–149. https://doi.org/10.1016/j.epsl.2016.03.050

Syracuse, E. M., van Keken, P. E., & Abers, G. A. (2010). The global range of subduction zone thermal models. *Physics of the Earth and Planetary Interiors*, *183*(1–2), 73–90. https://doi.org/10.1016/j.pepi.2010.02.004

Taboada, A., Rivera, L. A., Fuenzalida, A., Cisternas, A., Philip, H., Bijwaard, H., et al. (2000). Geodynamics of the northern Andes: Subductions and intracontinental deformation (Colombia). *Tectonics*, *19*(5), 787–813. https://doi.org/10.1029/2000TC900004

Takei, Y. (1998). Constitutive mechanical relations of solid-liquid composites in terms of grain-boundary contiguity. *Journal of Geophysical Research: Solid Earth*, *103*(B8), 18183–18203. https://doi.org/10.1029/98JB01489

Takei, Y. (2002). Effect of pore geometry on *Vp/Vs*: From equilibrium geometry to crack. *Journal of Geophysical Research: Solid Earth*, *107*(B2), ECV6-1–ECV6-12. https://doi.org/10.1029/2001JB000522

Takei, Y., & Holtzman, B. K. (2009). Viscous constitutive relations of solid-liquid composites in terms of grain boundary contiguity: 1. Grain boundary diffusion control model. *Journal of Geophysical Research*, *114*(B6), B06205. https://doi.org/10.1029/2008JB005850

Tan, E. (2017). Mantle wedge serpentinization effects on slab dips. *Terrestrial, Atmospheric, and Oceanic Sciences Journal*, *28*(3), 259–269. https://doi.org/10.3319/TAO.2016.09.21.01

Tan, Y., Hu, J., Zhang, H., Chen, Y., Qian, J., Wang, Q., et al. (2020). Hydraulic fracturing induced seismicity in the southern Sichuan Basin due to fluid diffusion inferred from seismic and injection data analysis. *Geophysical Research Letters*, *47*(4), e2019GL084885. https://doi.org/10.1029/2019GL084885

Tao, J., Dai, L., Lou, D., Li, Z.-H., Zhou, S., Liu, Z., et al. (2020). Accretion of oceanic plateaus at continental margins: Numerical modeling. *Gondwana Research*, *81*, 390–402. https://doi.org/10.1016/j.gr.2019.11.015

Tetreault, J. L., & Buiter, S. J. H. (2012). Geodynamic models of terrane accretion:; Testing the fate of island arcs, oceanic plateaus, and continental fragments in subduction zones. *Journal of Geophysical Research*, *117*(B8), B08403. https://doi.org/10.1029/2012JB009316

Tetreault, J. L., & Buiter, S. J. H. (2014). Future accreted terranes: A compilation of island arcs, oceanic plateaus, submarine ridges, seamounts, and continental fragments. *Solid Earth*, *5*(2), 1243–1275. https://doi.org/10.5194/se-5-1243-2014

Thielmann, M., Rozel, A., Kaus, B. J. P., & Ricard, Y. (2015). Intermediate-depth earthquake generation and shear zone formation caused by grain size reduction and shear heating. *Geology*, *43*(9), 791–794. https://doi.org/10.1130/G36864.1

Thielmann, M., & Schmalholz, S. M. (2020). Contributions of grain damage, thermal weakening, and necking to slab detachment. *Frontiers in Earth Science*, *8*, 254. https://doi.org/10.3389/feart.2020.00254

Toussaint, J. F., & Restrepo, J. J. (2020). Tectonostratigraphic terranes in Colombia: An update. Second part: Oceanic terranes. In J. Gómez & A. O. Pinilla-Pachon (Eds.), *The geology of Colombia, volume 2 Mesozoic, Publicaciones Geológicas Especiales* (Vol. 36, pp. 237–260). Bogotá: Servicio Geológico Colombiano. https://doi.org/10.32685/pub.esp.36.2019.07

Uchida, N., Kirby, S. H., Okada, T., Hino, R., & Hasegawa, A. (2010). Supraslab earthquake clusters above the subduction plate boundary offshore Sanriku, northeastern Japan: Seismogenesis in a graveyard of detached seamounts? *Journal of Geophysical Research*, *115*(B9), B09308. https://doi.org/10.1029/2009JB006797

Ueki, K., & Iwamori, H. (2016). Density and seismic velocity of hydrous melts under crustal and upper mantle conditions. *Geochemistry, Geophysics, Geosystems*, *17*(5), 1799–1814. https://doi.org/10.1002/2015GC006242

van Keken, P. E., Wada, I., Abers, G. A., Hacker, B. R., & Wang, K. (2018). Mafic high-pressure rocks are preferentially exhumed from warm subduction settings. *Geochemistry, Geophysics, Geosystems*, *19*(9), 2934–2961. https://doi.org/10.1029/2018GC007624

Vargas, C. A., Idarraga-Garcia, J., & Salazar, J. M. (2015). Curie point depths in northwestern South America and the southwestern Caribbean Sea. In C. Bartolini & P. Mann (Eds.), *Petroleum geology and potential of the Colombian Caribbean Margin, AAPG Memoir* (Vol. 108, pp. 179–200). American Association of Petroleum Geologists. https://doi.org/10.1306/13531936M1083642

Vargas, C. A., & Mann, P. (2013). Tearing and breaking off of subducted slabs as the result of collision of the Panama Arc-Indenter with northwestern South America. *Bulletin of the Seismological Society of America*, *103*(3), 2025–2046. https://doi.org/10.1785/0120120328

Vargas, C. A., Ochoa, L. H., & Caneva, A. (2019). Estimation of the thermal structure beneath the volcanic arc of the Northern Andes by coda wave attenuation tomography. *Frontiers in Earth Science*, *7*, 208. https://doi.org/10.3389/feart.2019.00208

Vogt, K., & Gerya, T. V. (2014). From oceanic plateaus to allochthonous terranes: Numerical modeling. *Gondwana Research*, *25*(2), 494–508. https://doi.org/10.1016/j.gr.2012.11.002

von Bargen, N., & Waff, H. S. (1986). Permeabilities, interfacial areas and curvatures of partially molten systems: Results of numerical computations of equilibrium microstructures. *Journal of Geophysical Research: Solid Earth*, *91*(B9), 9261–9276. https://doi.org/10.1029/JB091iB09p09261

von Bargen, N., & Waff, H. S. (1988). Wetting of enstatite by basaltic melt at 1350°C and 1.0- to 2.5-GPa pressure. *Journal of Geophysical Research: Solid Earth*, *93*(B2), 1153–1158. https://doi.org/10.1029/JB093iB02p01153

Wada, I., & Wang, K. (2009). Common depth of slab-mantle decoupling: Reconciling diversity and uniformity of subduction zones. *Geochemistry, Geophysics, Geosystems*, *10*, Q10009. https://doi.org/10.1029/2009GC002570

Wada, I., Wang, K., He, J., & Hyndman, R. D. (2008). Weakening of the subduction interface and its effects on surface heat flow, slab dehydration, and mantle wedge serpentinization. *Journal of Geophysical Research: Solid Earth*, *113*(B4), B04402. https://doi.org/10.1029/2007JB005190

Wagner, L. S., Jaramillo, J. S., Ramírez-Hoyos, L. F., Monsalve, G., Cardona, A., & Becker, T. W. (2017). Transient slab flattening beneath Colombia. *Geophysical Research Letters*, *44*(13), 6616–6623. https://doi.org/10.1002/2017GL073981

Waldhauser, F. (2001). *HypoDD—A program to compute double-difference hypocenter locations (Open-File Report 01-113)*. U.S. Geological Survey. Retrieved from https://pubs.usgs.gov/of/2001/0113/pdf/hypoDD.pdf

Waldhauser, F., & Ellsworth, W. L. (2000). A double-difference earthquake location algorithm: Method and application to the northern Hayward Fault, California. *Bulletin of the Seismological Society of America*, *90*(6), 1353–1368. https://doi.org/10.1785/0120000006

Waldhauser, F., & Ellsworth, W. L. (2010). HypoDD (version 1.3) [Software]. *Lamont-Doherty Earth Observatory*. Retrieved from https://www.ldeo.columbia.edu/~felixw/hypoDD.html

Waldhauser, F., & Schaff, D. (2007). Regional and teleseismic double-difference earthquake relocation and waveform cross-correlation and global bulletin data. *Journal of Geophysical Research*, *112*(B12), B12301. https://doi.org/10.1029/2007JB004938

Wang, D., Liu, T., Chen, T., Qi, X., & Li, B. (2019). Anomalous sound velocities of antigorite at high pressure and implications for detecting serpentinization at mantle wedges. *Geophysical Research Letters*, *46*(10), 5153–5160. https://doi.org/10.1029/2019GL082287

Wang, D., Liu, X., Liu, T., Shen, K., Welch, D. O., & Li, B. (2017). Constraints from the dehydration of antigorite on high-conductivity anomalies in subduction zones. *Scientific Reports*, *7*(1), 16893. https://doi.org/10.1038/s41598-017-16883-4

Wang, Y., Forsyth, D. W., Rau, C. J., Carriero, N., Schmandt, B., Gaherty, J. B., & Savage, B. (2013). Fossil slabs attached to unsubducted fragments of the Farallon plate. *Proceedings of the National Academy of Sciences*, *110*(14), 5342–5346. https://doi.org/10.1073/pnas.1214880110

Wark, D. A., Williams, C. A., Watson, E. B., & Price, J. D. (2003). Reassessment of pore shapes in microstructurally equilibrated rocks, with implications for permeability of the upper mantle. *Journal of Geophysical Research: Solid Earth*, *108*(B1), 2050. https://doi.org/10.1029/2001JB001575

Weber, M., Duque, J. F., Hoyos, S., Cárdenas-Rozo, A. L., Gómez, J., Wilson, R. (2020). The Combia volcanic province: Miocene post-collisional magmatism in the northern Andes. In J. Gómez & D. Mateus-Zabala (Eds.), *The geology of Colombia, volume 3 Paleogene-Neogene, Publicaciones Geológicas Especiales* (Vol. 37, pp. 355–394). Servicio Geológico Colombiano. https://doi.org/10.32685/pub.esp.37.2019.12

Wells, R., Bukry, D., Friedman, R., Pyle, D., Duncan, R., Haeussler, P., & Wooden, J. (2014). Geologic history of Siletzia, a large igneous province in the Oregon and Washington Coast Range: Correlation to the geomagnetic polarity time scale and implications for a long-lived Yellowstone hotspot. *Geosphere*, *10*(4), 692–719. https://doi.org/10.1130/GES01018.1

White, L. T., Rawlison, N., Lister, G. S., Waldhauser, F., Hejrani, B., Thompson, D. A., et al. (2019). Earth's deepest earthquake swarms track fluid ascent beneath nascent arc volcanoes. *Earth and Planetary Science Letters*, *521*, 25–36. https://doi.org/10.1016/j.epsl.2019.05.048

Worzewski, T., Jegen, M., Kopp, H., Brasse, H., & Taylor Castillo, W. (2011). Magnetotelluric image of the fluid cycle in the Costa Rican subduction zone. *Nature Geoscience*, *4*(2), 108–111. https://doi.org/10.1038/ngeo1041

Yin, A., & Harrison, T. M. (2000). Geologic evolution of the Himalayan-Tibetan Orogen. *Annual Review of Earth and Planetary Sciences*, *28*(1), 211–280. https://doi.org/10.1146/annurev.earth.28.1.211

Zapata, S., Cardona, A., Jaramillo, J. S., Patiño, A., Valencia, V., León, S., et al. (2019). Cretaceous extensional and compressional tectonics in the Northwestern Andes, prior to the collision with the Caribbean oceanic plateau. *Gondwana Research*, *66*, 207–226. https://doi.org/10.1016/j.gr.2018.10.008

Zapata-García, G., & Rodríguez-García, G. (2020). New contributions to the knowledge about the Chocó-Panamá Arc in Colombia, including a new segment south of Colombia. In J. Gómez & D. Mateus-Zabala (Eds.), *The geology of Colombia, volume 3 Paleogene-Neogene, Publicaciones Geológicas Especiales* (Vol. 37, pp. 417–450). Servicio Geológico Colombiano. https://doi.org/10.32685/pub.esp.37.2019.14

Zeiler, C., & Velasco, A. A. (2009). Seismogram picking error form analyst review (SPEAR): Single-analyst and institution analysis. *Bulletin of the Seismological Society of America*, *99*(5), 2759–2770. https://doi.org/10.1785/0120080131

Zhan, Z., & Kanamori, H. (2016). Recurring large deep earthquakes in Hindu Kush driven by a sinking slab. *Geophysical Research Letters*, *43*(14), 7433–7441. https://doi.org/10.1002/2016GL069603

Zhang, H., & Thurber, C. H. (2003). Double-difference tomography: The method and its application to the Hayward Fault, California. *Bulletin of the Seismological Society of America*, *93*(5), 1875–1889. https://doi.org/10.1785/0120020190

Zhang, H., Thurber, C. H., Shelly, D., Ide, S., Beroza, G. C., & Hasegawa, A. (2004). High-resolution subducting-slab structure beneath northern Honshu, Japan, revealed by double-difference tomography. *Geology*, *32*(4), 361–364. https://doi.org/10.1130/G20261.2

Zhang, N., Behn, M. D., Parmentier, E. M., & Kincaid, C. (2020). Melt segregation and depletion during ascent of buoyant diapirs in subduction zones. *Journal of Geophysical Research: Solid Earth*, *125*(2), e2019JB018203. https://doi.org/10.1029/2019JB018203

Zhao, S., Schettino, E., Merlini, M., & Poli, S. (2019). The stability and melting of aragonite: An experimental and thermodynamic model for carbonated eclogites in the mantle. *Lithos*, *324–325*, 105–114. https://doi.org/10.1016/j.lithos.2018.11.005

Zhu, G., Gerya, T. V., Yuen, D. A., Honda, S., Yoshida, T., & Connolly, J. A. D. (2009). Three-dimensional dynamics of hydrous thermal-chemical plumes in oceanic subduction zones. *Geochemistry, Geophysics, Geosystems*, *10*(11), Q11006. https://doi.org/10.1029/2009GC002625

References From the Supporting Information

Servicio Geológico Colombiano. (1993). Red Sismologica Nacional de Colombia [Dataset]. *International Federation of Digital Seismograph Networks*. https://doi.org/10.7914/SN/CM